1 Systemic inflammation recruits fast-acting anti-inflammatory innate myeloid progenitors

2 from BM into lymphatics

- Juana Serrano-Lopez^{1*}, Shailaja Hegde^{1,2*}, Sachin Kumar¹, Josefina Serrano³, Jing Fang¹,
- 4 Ashley M. Wellendorf¹, Paul A. Roche⁴, Yamileth Rangel³, Léolène J. Carrington⁵, Hartmut
- 5 Geiger^{1,6}, H. Leighton Grimes⁷, Sanjiv Luther⁸, Ivan Maillard⁵, Joaquin Sanchez-Garcia³, Daniel
- 6 T. Starczynowski^{1,9}, Jose A. Cancelas^{1,2}
- ⁷ ¹Divisions of Experimental Hematology and ⁷Immunobiology, Department of Pediatrics,
- 8 Cincinnati Children's Hospital Medical Center, University of Cincinnati College of Medicine,
- 9 3333 Burnet Avenue, Cincinnati, OH 45229, USA.
- ² Hoxworth Blood Center, University of Cincinnati College of Medicine, 3130 Highland Avenue,
- 11 Cincinnati, OH 45219.
- ³ Dept. of Hematology, Hospital Reina Sofia, Avda. Menendez Pidal s/n, Cordoba 14004, Spain.
- ⁴ Center for Cancer Research, National Cancer Institute, 37 Convent Dr., Bethesda, MD 20892.
- ⁵ University of Pennsylvania Perelman School of Medicine, Philadelphia, PA 19104
- ⁶ Institute of Molecular Medicine, Ulm University, 89081 Ulm, Germany.
- ⁸ Center for Immunity and Infection, Department of Biochemistry, University of Lausanne, 1066
- 17 Epalinges, Switzerland
- ⁹ Department of Cancer Biology, University of Cincinnati, 3125 Eden Avenue, Cincinnati, OH
- 19 45267.
- 20 * Both authors contributed equally.
- 21 Corresponding author:
- 22 Jose A. Cancelas MD, PhD
- 23 Hoxworth Blood Center and Division of Experimental Hematology and Cancer Biology
- 24 Cincinnati Children's Hospital Medical Center
- 25 University of Cincinnati College of Medicine
- 26 3333 Burnet Ave., Cincinnati, OH, 45229, USA
- 27 Tel: +1-513-558-1324; Fax: +1-513-558-1522
- 28 E-mail: jose.cancelas@uc.edu; jose.cancelas@cchmc.org

29 ABSTRACT

30

31	Innate immune cellular effectors are actively consumed during systemic inflammation but the
32	systemic traffic and the mechanisms that support their replenishment remain unknown. Here we
33	demonstrate that acute systemic inflammation induces the emergent activation of a previously
34	unrecognized system of rapid migration of granulocyte-macrophage progenitors and committed
35	macrophage-dendritic progenitors, but not other progenitors or stem cells, from bone marrow
36	(BM) to lymphatic capillaries. The progenitor traffic to the systemic lymphatic circulation is
37	mediated by Ccl19/Ccr7 and is NF κ B independent, Traf6/I κ B-kinase/SNAP23 activation which
38	is responsible for the secretion of pre-stored Ccl19 by a subpopulation of CD205 ⁺ /CD172a ⁺
39	conventional dendritic cells type 2 (cDC2) and upregulation of BM myeloid progenitor Ccr7
40	signaling. The consequence of this progenitor traffic is anti-inflammatory with promotion of early
41	survival and initiation of replenishment of lymph node cDC.

42

44 INTRODUCTION

45

Bacterial infections represent one of the major threats for the human immune system 46 and can lead to sepsis or death (Martin et al., 2003). A functional immune response is a key 47 factor to control the outcome of bacterial infections. Therefore, the human immune system has 48 evolved several effector mechanisms to fight bacterial infections which involve the innate and 49 50 the adaptive arms of the immune system. Antigen presentation is an essential mechanism of 51 activation that requires crosstalk between the innate and adaptive immune system to fight 52 bacterial infections. Dendritic cells are short-lived professional antigen presenting cells (APC) 53 and their life span is further reduced during the inflammatory response to pathogens (Kamath et al., 2002). Upon inflammation, primed APC thus need to be replaced. 54

55 During inflammation, systemic signals alert and activate bone marrow (BM) myeloid differentiation (Baldridge et al., 2010; Essers et al., 2009; Nagai et al., 2006). Inflamed 56 57 secondary lymphoid organs such as lymph nodes (LN) recruit antigen-presenting dendritic cells (DC) (Legler et al., 1998; Luther et al., 2000; Saeki et al., 1999), while pathogen-associated 58 molecular pattern signals (PAMPs) trigger migration of tissue-resident DC to the LN (Kaisho and 59 Akira, 2001; Sallusto and Lanzavecchia, 2000). Circulation of hematopoietic stem cells and 60 61 progenitors (HSC/P) that enter the lymphatic vessels from the peripheral blood (PB) with ability 62 to amplify APCs has been described (Massberg et al., 2007). However, the circuits used by 63 these HSC/P populations, their characterization and the cellular and molecular mechanisms that regulate this traffic in inflammatory conditions have not been addressed in detail. 64

Lymphatics form part of an open circulatory system that drains cells and interstitial fluid from tissues. Recently, bone lymphatic endothelial cells have been shown to arise rapidly from pre-existing regional lymphatics in inducible bone-expressing *Vegfc* transgenic mice through Vegfr3, osteoclast activation and bone loss (Hominick et al., 2018; Monroy et al., 2020). Acute endotoxemia is associated with osteoclast activation and bone loss (Hardy and Cooper, 2009; Nason et al., 2009). We postulated the pre-existence of an anatomical and functional patent

71 circuit that communicates BM and lymphatic tissues that can be induced upon severe

72 inflammatory conditions like endotoxemia.

73 Our work identifies an emergent traffic of DC-biased myeloid progenitors through direct 74 transit from BM to bone lymphatic capillaries. This traffic is highly activated in endotoxic 75 inflammation. In human reactive lymphadenitis or just after a single immune endotoxic 76 challenge, such as following lipopolysaccharide (LPS) stimulation in mice, a massive 77 mobilization of myeloid progenitors from the BM to lymph and retention in the LN takes place. 78 The mobilization is rapid, prior to their appearance in PB. LPS simultaneously induces cellautonomous Ccr7 expression on granulo-macrophage progenitors (GMP) and macrophage-79 dendritic progenitors (MDP), and a non-cell autonomous myeloid cell-dependent secretion of 80 Ccl19 in the LN. In vivo blockade of LPS signaling in mature myeloid cells, deletion of 81 82 hematopoietic Ccl19 or neutralization of Ccr7 completely abrogated the GMP/MDP migration 83 from the BM to the LN and increased acute inflammation associated mortality. Moreover, genetic and pharmacological approaches revealed that Traf6-Irak1/4-Ubc13-IkB kinase (IKK) 84 signaling mediates NF-kB-independent-SNAP23 phosphorylation and secretion of pre-formed 85 86 Ccl19 from a specific population of conventional dendritic cells (cDC). These findings indicate 87 that inflammation results in mobilization of cDC-forming cells directly from the BM to the lymph and LN. As such, emergent myeloid lineage mobilization from the BM to lymph may be 88 89 important in inflammation by acutely replenishing antigen-presenting cells in lymph tissues and 90 impairing the inflammatory signaling responsible for mortality in endotoxemia.

91

93 RESULTS

94 Inflammation associates with emergent migration of myeloid progenitors, but not HSC,

95 from BM to lymphatics.

96 To determine whether there is a circulation of HSC/P to human LN, we prospectively analyzed the presence of side population (SP) cells in LN biopsies (Figure S1A) obtained from 97 98 lymphadenitis and lymphoma patients at diagnosis. Human and murine SP cells, with ability to 99 extrude the dye Hoechst 33342 through upregulated activity of multidrug resistance protein 100 complexes (Zhou et al., 2001) in BM and other tissues (Brusnahan et al., 2010; Challen and 101 Little, 2006; Goodell et al., 1996) are enriched in long-term reconstituting HSC and other more 102 committed populations of progenitors (Matsuzaki et al., 2004; Weksberg et al., 2008). We found 103 a SP population at a frequency higher than 0.01% in 36 out of 64 LN biopsies (53.12%). However, the content of SP cells in the LN did correlate with the LN histological diagnosis. The 104 105 elevated frequency of SP cells in LN did correlate with the LN histological diagnosis (Figure 1A) 106 but not to the anatomical location of the lymphadenopathy (Figure S1B; Table S1). The accumulation of SP cells was significantly higher in LN from lymphadenitis patients than in 107 108 lymphoma patients. Further dissection based on histological classifications by independent 109 pathology analysis resulted in the lymphadenitis specimens being sorted into distinct histological 110 categories which corresponded to follicular lymphadenitis with paracortical predominance (FL), granulomatous lymphadenitis (GL), and lymphadenopathies with histological or molecular 111 evidence of viral etiology (viral lymphadenitis, VL). Interestingly, FL and GL LN contained a 112 113 median of 0.2% SP cells with a range from <0.01% to $\sim40\%$, which was significantly higher than 114 the content of SP cells in VL, Hodgkin's lymphoma, and non-Hodgkin's lymphoma LN (Figure 1A; Figure S1A, Table S1). The existence of myeloid-committed hematopoietic 115 116 progenitors was confirmed in myeloid colony-forming cell unit (CFU) assays (Figure S1C) 117 performed on samples from patients with FL. These data show that non-viral inflammatory 118 lymphadenitis results in a significantly increased frequency of primitive hematopoietic cells in LN, while it does not reveal the type of progenitor cells. To confirm whether LN SP cells indeed 119

120 contained HSC/P, we first sorted LN SP cells from patients with reactive lymphadenitis and 121 plated them in semisolid cultures containing rhIL-3, rhIL-6 and rhSCF cytokines CFU analysis demonstrated that SP cells were indeed capable of producing myeloid colonies (Figures S1D), 122 123 while non-SP cells were devoid of measurable CFU-forming ability (data not shown). 124 Immunophenotypic analysis of SP-derived progenitors was also consistent with enrichment of a 125 heterocellular population of CD34 and CD133 expressing granulocyte-, granulocytemacrophage-, and cDC-biased progenitors (Bornhauser et al., 2005; Gorgens et al., 2013) 126 (Figure S1D). The vast majority of CD45⁺/CD34⁺ cells co-expressed CD133⁺, and the 127 128 CD45⁺/CD34⁻ population was split ~50:50 into CD133⁺ and CD133⁻ cells (FigureS1D). In combination, these data show the accumulation of a myeloid-committed HSC/P population in 129 human lymphadenitis. Adult inflammatory LN tissues therefore contain an increased number of 130 myeloid-committed HSC/P. This increase can result from either the recruitment of these cells to 131 LN via the bloodstream or the expansion of otherwise rare and already resident myeloid-132

133 committed HSC/P in these LN.

The release of HSC/P from BM into the bloodstream follows circadian cycles (Mendez-134 135 Ferrer et al., 2008) controlled by the activity and fate of inflammatory cells (Casanova-Acebes et al., 2013; Chang et al., 2014). We postulated that if inflammation is responsible for the 136 recruitment of HSC/P to the LN and possibly other organs, we should be able to recapitulate the 137 process of BM egression, migration, and organ retention, in an inflammatory murine model 138 139 wherein the HSC/P migration process is highly conserved. Since the largest content of HSC/P in 140 human LN was found in biopsies from patients with lymphadenitis, we generated a mouse 141 model of Gram-negative sepsis by injection of *E. coli* LPS into C57BI/6 mice at the early timepoint of the circadian HSC/P mobilization cycle (zeitgeber time, ZT) (Bellet et al., 2013) 142 143 (Figure1B). E. coli LPS is able to activate a large number of Toll-like receptors (TLR), which 144 result in high-level activation of the inflammatory signaling cascade (Beutler and Rietschel, 2003). LPS is also a well-known inducer of HSC/P mobilization to PB(Cline and Golde, 1977; 145 Velders et al., 2004; Vos et al., 1972; Vos and Wilschut, 1979). In our experiments, the 146

147 circadian mobilization pattern of HSC/P in the PB was severely modified by the administration of 148 LPS, with the increase in HSC/P appearing later and peaking at ZT10, 6 hours postadministration (Figure1C), coincident with an increased neutrophil count in the PB (Figure 149 **S1E**). We observed similar kinetics of an increased numbers of HSC/P in the highly 150 151 vascularized kidney and liver tissues after LPS administration (Figure 1D-E), suggesting that 152 the presence of HSC/P in these tissues closely paralleled their presence in the PB. Interestingly, LPS did not elicit a significant change in the level of splenic HSC/P within the first 12 hours after 153 154 inflammation (Esplin et al., 2011; Wright et al., 2001) (Figure 1F).

155 Notably, when the HSC/P content was reduced in the BM, the kinetics of their subsequent mobilization to the PB was discordant. The BM HSC/P content decreased, which 156 supports the migratory nature of the increased HSC/P in the PB (Figure 1G); yet the nadir of 157 158 the BM HSC/P content occurred as early as 3 hours after LPS administration (at ZT7), returning 159 to normal values by 6 hours (ZT10, Figure 1G). The time lapse between the loss of retention of HSC/P in the BM and their presence in the PB circulation suggested that the migration of 160 HSC/P from the BM to the PB required an intermediate step of circulation through other tissues. 161 162 Based on an earlier description of a lymphatic circulation of HSC/P (Massberg et al., 2007), we hypothesized that this delay in the appearance of HSC/P in the PB was due to an intermediate 163 transit of HSC/P through the lymphatic circulation. Indeed, the lymphatic circulation in LPS-164 treated animals did show a significant increase in the levels of circulating HSC/P in the LN and 165 166 the thoracic duct compared to controls that closely mirrored the decline of HSC/P in the BM

167 (Figures 1H-I).

We next characterized the type of primitive cell populations migrating into the LN via the lymphatic circulation. We first analyzed whether the content of immunophenotypically identifiable BM HSC populations changed concomitantly with the progenitor population changes previously described. LPS induced expansion of BM Lin⁻/c-kit⁺/Sca-1⁺ (LSK) and immunophenotypically identified long-term (LT)-HSC, short-term (ST)-HSC and multipotential progenitors (MPP) populations at later time points (Z10-ZT16) (**Figures S1F and S1H-K**) with

174 no changes in the BM HSC content by ZT7, suggesting a differential effect of LPS signaling on 175 the HSC population. Interestingly, the reduction in the BM content of progenitors was not homogenous throughout the hematopoietic progenitor populations. Confirming the earess of BM 176 CFU-GM described above, the GMP population was significantly decreased by ZT7 (Figures 177 178 **S1G, L**), while the content of immunophenotypically defined common myeloid progenitors 179 (CMP) only declined by ZT10 (Figures S1G, M), and the megakaryocyte-erythroid progenitor (MEP) content was increased (Figures S1G, N), resulting in no significant net changes in the 180 content of BM Lin⁻/c-kit⁺/Sca1⁻ (LK) cells (Figures S1G, O). 181

182 Functional in vivo assays of LN cell suspensions obtained at ZT7 demonstrated that the accumulation of progenitors in LN did not contain any significant numbers of long-term or 183 medium-term repopulating HSC. The analysis of competitive-repopulating units (CRU) in the LN 184 185 (Figure S2A) demonstrated that inflamed LN did not contain increased levels of repopulating 186 cells by ZT7 (Figure S2B). LN contained a transient, ST-myelopoietic progenitor population without medium- or long-term multilineage repopulation ability (Figure S2C). Lineage analysis 187 of donor-derived circulating cells demonstrated no significant change in T-cell transfer (Figure 188 189 S2D), and a diminished transfer of B-cells into the lethally irradiated recipients (Figure S2E) indicating the presence of adoptively transferred lymphoid cells and the absence of mobilization 190 of competent lymphoid progenitors to the inflamed LN. Furthermore, LN SP cells from LPS-191 treated mice are enriched in LK cells and depleted in LSK cells (Figure S2F). LN SP cells 192 193 contain exclusively ST-repopulating progenitors with the ability to differentiate into myeloid cells 194 (data not shown) and are depleted from any significant 8-16 weeks engrafting HSC, as assessed using CRU assays (Figures S2F-G), unlike their BM SP counterparts which are 195 196 enriched in LSK cells and LT-repopulating activity (Figures S2F, H). These results confirmed 197 that, similar to human inflammatory LN, the LN SP cells from mice treated with E. Coli LPS 198 accumulate in inflamed LN, contain progenitors, and are depleted of stem cell activity. Altogether, these data indicate that LPS induces a selective lymphatic circulation of myeloid 199 committed progenitors, but not other types of HSC/P populations. 200

201 To explore the nature of the circuit of the myeloid progenitor migration to LN, we first 202 analyzed the ability of HSC/P to seed LN in non-myeloablated mice. For this experiment, we labeled C57BI/6-BM-derived lineage negative (Lin⁻) cells containing the HSC/P fraction with the 203 lipophilic dye 1,1'-dioctadecyl-3,3,3',3'-tetramethylindocarbocyanine perchlorate (Dil), and 204 205 adoptively transferred them into un-manipulated lymphatic vessel reporter Lyve1-eGFP mice. Lyve1-GFP knock-in mice display enhanced green fluorescent protein (eGFP) fluorescence 206 driven by the promoter/enhancer of the lymphatic vessel hyaluronan receptor 1 Lyve-1 207 208 identifying lymphatic endothelial cells (Pham et al., 2010). We analyzed the 17-hour homing of 209 Lin⁻ cells to the BM and LN (Figure 2A). The homing of cells to the BM in mice treated with LPS 210 was reduced by ~65% compared with their vehicle-treated counterparts (Figure 2B). To determine whether Lin⁻/Dil⁺ homed cells leave BM in response to LPS, we first determined the 211 existence of transcortical vessels (Figure 2C)(Gruneboom et al., 2019) and the presence of 212 213 lymphatic vasculature inside the bone by two-photon microscopy in mice either treated with PBS 214 or LPS (Figures 2D-E and Movies S1-2). Lyve1-GFP knock-in mice revealed that the bone of LPS-treated animals contains a Lyve1+ network, which was only rarely identified in PBS-treated 215 mice (Figure 2D), suggesting that LPS induced inflammation may upregulate the expression of 216 217 the hyaluronan receptor Lyve1 and render patent a pre-existing network of Lyve1+ bone cells. Interestingly, Lin/Dil⁺ homed cells were located closer to the endosteum in response to LPS at 218 219 as early as 1.5 hours after administration of LPS (Figure 2E). Quantification of the distance of 220 Lin⁻/Dil⁺ homed cells to endosteum area showed significant differences between PBS and LPS 221 treatment, indicating increased proximity to the endosteum area after LPS (Figure 2F). We 222 found, albeit at a very low frequency, tiny lymphatics scattered and projected inside the bone 223 (Figure 2G and Movie S3). On the other hand, the seeding of BM-derived Lin⁻/Dil⁺ cells into LN 224 increased ~3-fold which mirrored the decline in BM homing (Figure 2H-J). Histological analysis 225 of BM-derived Lin/Dil⁺ cells within the LN by confocal microscopy showed that the migrated HSP/C are spatially positioned in the cortex area surrounding primary follicles (Figure 2I), 226 consistent with localization in T-cell zone for antigen presentation. These findings strongly 227

suggest that the rapid egress of hematopoietic progenitors from BM during inflammation may

indeed occur through bone lymphatics draining into LN.

230

231 Systemic inflammation recruits dendritic cell-committed phenotypic progenitors to LN

232 To determine the potential of the myeloid progenitors mobilized to the LN, we further determined their in vitro and in vivo differentiation profile. To this end we analyzed the 233 234 differentiation capabilities of LN myeloid progenitors in specific-cytokine driven clonal assays in methylcellulose assays. The majority of the differentially accumulated myeloid progenitors in LN 235 by 3 hours post-administration of LPS were granulocyte-macrophage progenitors (CFU-GM) 236 and in a much lesser degree unipotent granulocyte progenitors (GPs, CFU-G) with no 237 differential accumulation of unipotent macrophage progenitors (MPs, CFU-M) (Figure 3A). 238 239 Next, we investigated whether GMP were able to home and migrate to LN after in vivo administration of LPS. For this purpose, we adoptively transferred sorted β -actin/eGFP 240 transgenic GMPs into congenic mice. Transgenic GMPs were allowed to home to the BM and 241 242 after 17 hours recipient mice were treated with a single dose of LPS or vehicle control. On day 7 after PBS or LPS administration, murine BM and LN were analyzed for donor-derived 243 granulocytes (Gr1⁺⁺/CD11b⁺/CD11c^{neg}), macrophages (Gr1^{dim}/CD11b⁺/CD11c^{neg}) and cDC 244 245 (Gr1^{neg}/CD11b⁺/CD11c⁺) by flow cytometry (**Figure 3B**). We found that LPS induced differential 246 donor-derived specific GMP differentiation towards the formation and retention of cDC in LN 247 (Figure 3C), but not in the BM (Figure 3D). The content of macrophages and granulocytes did not significantly change with LPS in either LN or BM (Figures 3C-D) confirming the specific 248 249 nature of the cDC differentiation of mobilized GMP in LPS-treated mice, similar to our 250 observations in human lymphadenitis.

To elucidate whether the LN cDC content was dependent on migration of committed cDC precursors opposed to local specification of migrated macrophages or macrophage progenitors, we analyzed the migration of macrophage-dendritic precursors (MDP). BM MDP is a progenitor population that can differentiate into monocytes/macrophages or directly into cDCs

without intermediate macrophage specification (Fogg et al., 2006; Geissmann et al., 2003;

Waskow et al., 2008). MDP are characterized by high expression of the chemokine receptor
Cx3cr1, c-fms (CD115) and Flt3, and intermediate expression of c-Kit. Serial gating of Lineage⁻
/Cx3cr1⁺⁺/c-Kit^{int} cells (Figure 3E, P2) showed an ~3-fold accumulation of CD115⁺⁺/FLT3⁺⁺ cells
in LN and a concomitant 65% depletion in the BM, as early as 3 hours after LPS administration
(Figures 3F-G and Figures S3A-B). In the absence of significant changes in the LN content of
macrophages, these data demonstrate that LPS-induced systemic inflammation results in robust
and specific recruitment of phenotypic GMP that are BM cDC committed progenitors to the LN.

263

264 Myeloid progenitor migration to LN is Traf6-dependent and NF-κB-independent.

Immune cells and HSC/P express TLR (Beutler and Rietschel, 2003; Nagai et al., 2006; 265 266 Takeuchi and Akira, 2010) which act as microorganism sensors. LPS stimulation of TLR recruits 267 MyD88 and TRIF through the canonical and endosomal pathways respectively. Both adaptors subsequently recruit TRAF6, which acts as the molecular hub of both signaling branches (Akira 268 et al., 2001; Kawai and Akira, 2006). To determine whether Traf6 deficiency might affect the 269 270 migration of HSC/P in response to LPS, we exploited an animal model in which Traf6 is deleted 271 only in hematopoietic cells (Kobayashi et al., 2003) (Figure 4A, Figure S3C). LN from Mx1Cre;WT chimeric mice after LPS administration (at ZT7, corresponding with the peak of 272 progenitor content in LN, Figure 1H) revealed a 3-fold increase in the frequency of CFU-GM. 273 This increase was completely abrogated by the deficiency of Traf6 in hematopoietic cells 274 (*Mx1Cre:Traf6*^{Δ/Δ} animals, **Figure 4B**) indicating that the signals which result in CFU-GM 275 mobilization to LN are mediated by hematopoietic Traf6. 276

Although HSC/P respond directly to PAMPs such as LPS (Nagai et al., 2006; Zhao et al., 2014), direct Gram-negative infection-derived LPS sensing by HSC/P does not play an essential role in emergency granulopoiesis, but rather requires TLR4-dependent signals within the microenvironment (Boettcher et al., 2012; Kwak et al., 2015). To further test whether the hematopoietic Traf6-dependent response to LPS resulting in mobilization of GMP from the BM

282 to the LN by ZT7 is indeed cell autonomous and not determined by the microenvironment, we 283 used the conditional Traf6-deficiency model and analyzed the in vitro migration of myeloid progenitors towards chemoattractant gradients generated by LPS-stimulated BM or LN cells in 284 assays designed to identify the hematopoietic cell population affected by LPS (Figures 4C, E, 285 **G**). We found that the cell-autonomous deficiency of Traf6 resulted in a relative decrease in 286 287 migration of ~40% (Figure 4D) of BM myeloid progenitors in presence of LPS, indicating that Traf6 is required for LPS-dependent cell-autonomous BM myeloid progenitor migration. 288 289 Interestingly, analysis of non-cell autonomous migration of BM myeloid progenitors 290 demonstrated that LN-derived cells generated more potent chemoattractant signals resulting in 291 a much larger migration of WT BM myeloid progenitors (5-fold higher, ~30%) during the same period (Figures 4E-F), which was drastically diminished (~50% reduction) by Traf6-deficiency in 292 293 LN cells, but not when using control BM cells as chemoattractant source (Figures 4E-F). These 294 data indicate that although LPS-mobilized myeloid progenitors depend on both cell-autonomous 295 and non-cell autonomous Traf6-dependent signals, the chemoattractant gradient generated by LPS on LN cells is the predominant effect responsible for Traf6-dependent myeloid progenitor 296 297 migration.

To delineate the resident LN population to cause the migration of GMPs into the LN, we 298 isolated T-cells (CD3e⁺), B-cells (B220⁺) and myeloid cells (CD11b⁺) from LN of WT or Traf6^{Δ/Δ} 299 300 mice and layered input cell equivalents on the bottom of the chamber with LPS, as in the 301 previous experiments (Figure 4G). Although only ~1% of LN cells are myeloid, we observed that LN CD11b⁺ cells, but not B or T cells, from Traf6^{Δ/Δ} mice can recapitulate the same 302 reduction of progenitor migration achieved by complete LN tissue (Figure 4H). To confirm that a 303 304 Traf6-dependent signaling in LN CD11b+ cells is responsible for myeloid progenitor mobilization 305 and eliminate the possible inflammatory effect of previous treatment with polyI:C in Mx1-Cre Tg mice, we crossed *Traf6^{flox/flox}* mice with *LysM-Cre* transgenic mice(Clausen et al., 1999; Cross et 306 al., 1988) and analyzed the migration to LN after LPS administration in mature myeloid lineage-307 specific Traf6 deficient (LysM-Cre;Traf6^{flox/flox}) mice. Mature myeloid lineage-specific deletion of 308

309 Traf6 abrogated the migration of myeloid progenitors to LN in response to LPS (Figure 4I). A 310 major consequence of the deficiency of Traf6 in mature myeloid lineage-specific cells was an increase in the endotoxemia dependent mortality (Figure 4J) indicating that Traf6 expression in 311 312 mature myeloid cells is required for both migration of myeloid progenitors to LN and protection 313 of the inflammatory cytokine storm responsible for LPS-induced death. Altogether, these data 314 indicate that LPS/Traf6 signaling is required for migration of myeloid progenitors through 315 predominantly long-range acting, mature myeloid lineage-dependent chemoattractant signals and that LPS/Traf6 signaling in LysM⁺ cells is protective against endotoxin-induced 316

317 inflammation.

318 Activation of TLRs conserves inflammatory pathways which culminate in the activation of the NF-κB transcription factors(Karin and Greten, 2005). The LPS binds TLR4/MD2 complexes 319 320 on the cell surface, and through a series of adaptors and kinases recruits Traf6. By an E3 321 ligase-dependent mechanism, Traf6 activates the IkB kinase (IKK) complex, which initiates IkBa degradation. Subsequent nuclear translocation of NF-KB transcription factors results in the 322 323 expression of cytokine and chemokine genes. To determine whether emergent NF-kB signaling 324 is responsible downstream of LPS/Traf6 for the LPS-induced LN migratory effect of myeloid progenitors, we overexpressed a degradation-resistant mutant of IkBa (IkBa super-repressor 325 $[I \kappa B \alpha_{SR}]$), in primary murine progenitors, which were then differentiated into macrophages/cDC 326 by macrophage colony-stimulating factor (M-CSF)(O'Keeffe et al., 2010) (Figure S3D). 327 328 Analysis of LPS-driven migration in vitro (Figure S3E) demonstrated that the expression of 329 IkBase does not reduce the effect of LPS on the migration of myeloid progenitors towards LPS-330 stimulated macrophages/cDC (Figures S3F-G), indicating that NF-kB transcription factors are dispensable for myeloid progenitor migration. In contrast, inhibition of intracellular protein traffic 331 332 using monensin dramatically decreased myeloid precursor migration (Figures S3F-G), 333 suggesting that intracellular protein trafficking is necessary for the migration phenotype. Collectively, these data indicate that LPS-induced myeloid progenitor migration occurs through 334 an NF-kB-independent, intracellular protein traffic-dependent pathway, and suggests that the 335

336 progenitor mobilizing effect of LPS may not require transcriptional activation, depending rather

337 on the intracellular traffic of secreted proteins.

338

339 Myeloid progenitors home into LN in a CCL19/CCR7 dependent fashion but

340 independently of L-selectin

341 The secretome of myeloid cells includes multiple cytokines/chemokines with short- and long-range activities on activation, proliferation, survival, differentiation, and migration of target 342 cells. Specifically, secreted chemokines stimulate migration of target cells following chemokines 343 344 to the areas of highest concentration. It has been described that hematopoietic progenitor migration is dependent on Cxcl12 gradients (Greenbaum et al., 2013; Mendez-Ferrer et al., 345 2010). However, by ZT7, LPS induced upregulation of Cxcl12 expression in BM, but not in LN, 346 347 indicating that Cxcl12 tissue concentrations per se could not explain the mechanism of 348 migration to LN (Figure S4A). An array of tests on secreted chemokines and cytokines and demonstrated distinct secretome signatures between BM and LN tissues after LPS 349 350 administration (Figures S4B-N). Several myeloid cell cytokines and chemokines with ability to 351 recruit and differentiate macrophages and cDC were found to be upregulated in the extracellular 352 fluid of LN rather than BM as early as one hour after LPS challenge (Figure S4C-J). However, 353 none of these candidate cytokines/chemokines were found to consistently generate a differential tissue concentration in vivo between LN and BM at both ZT5 and ZT7 (Figure S4B). Similar to 354 355 Cxcl12, some cytokines/chemokines with potential chemoattractant ability were also found to be 356 upregulated in BM rather than in LN or in both tissues similarly (Figure S4K-N). The lack of in vivo tissue differential levels strongly suggested that these BM-derived cytokines or chemokines 357 were unlikely to be responsible for the attraction of BM myeloid progenitors to the LN. 358

The C-C chemokine receptor type 7 (Ccr7) ligand macrophage-inflammatory protein (MIP)-3b/Ccl19 has been reported as a chemoattractant for BM and cord blood CD34⁺ cells *in vitro*, mainly CFU-GM (Kim et al., 1998). Analysis of Ccl19 in the extracellular fluid of the femoral cavity, LN, and plasma, demonstrated that *in vivo* administration of LPS promotes a

363 secretion of Ccl19 in LN when compared with BM and PB (Figure 5A). This differential 364 secretion is specific to Ccl19 since Ccl21, a highly-related chemokine, did not show the formation of similar differential tissue concentrations in LN after LPS administration (Figure 365 S5A). Ccl19 is secreted by LN myeloid cells after LPS stimulation and depends on Traf6 366 367 expression (Figure S5B). Ccr7-mediated signals control the migration of immune cells to 368 secondary lymphoid organs such as LN, facilitating efficient surveillance and targeted cellular response (Forster et al., 2008). Also, LPS upregulates membrane Ccr7 expression on cDC and 369 370 their committed progenitors (Schmid et al., 2011). We therefore hypothesized that LN-trafficking 371 of phenotypic GMP/MDP is regulated by Ccr7, and that therefore the Ccl19/Ccr7 axis might 372 explain the coexistence of cell-autonomous and non-cell autonomous mechanisms required for GMP migration from the BM to LN in response to LPS. To test our hypothesis, we first analyzed 373 whether the specific deficiency of either Ccl19 or Ccr7 modified the level of progenitor migration 374 375 to LN. To prevent the interference of long-term deficiencies of Ccl19 and Ccr7 expression 376 described in deficient murine models (Forster et al., 1999; Mori et al., 2001), we performed short-term in vivo neutralization of Ccl19 ligand or the Ccr7 receptor by using specific antibodies 377 or isotype controls (Figure 5B) and determine the content of CFU-GM in LN after LPS 378 379 challenge or PBS control. We administered an anti-Ccl19 and an anti-Ccr7 neutralizing antibody 380 (or their controls) twice within 15 hours before LPS administration. We found a dramatic 381 reduction (>90%) in the number of CFU-GM in the LN of LPS-, anti-Ccl19 treated animals by ZT7 (Figure 5C). Also, we confirmed that Ccr7-expressing GMP in BM rapidly decreased in 382 383 response to LPS and increased in local LN (Figures S5D-F). The abrogation of accumulation 384 of progenitors in LN was reproduced by the administration of anti-Ccr7 (Figure 5D). Noteworthy, 385 the administration of anti-Ccr7 phenocopied the effect of Traf6 deficiency in LysM⁺ cells by 386 decreasing the latency to death or increasing the mortality rate of mice treated with lethal 387 (Figure 5E) or sublethal (Figure 5F) doses of LPS in the first hours after LPS administration, respectively. Second, we analyzed the membrane expression of Ccr7 on BM-derived GMP, 388 CMP and MEP from *Mx1Cre;WT* or *Mx1Cre;Traf6*^{4/2} mice, with or without LPS stimulation. 389 390 Membrane Ccr7 levels were significantly upregulated as early as 1 hour after LPS

administration on GMP in LPS-treated WT mice. Such upregulation was abrogated in LPS treated Traf6-deficient GMP (Figures S5G). Finally, we confirmed that hematopoietic chimeric

- 393 Ccl19^{-/-} animals did not mount a migratory response of myeloid progenitors from BM to LN in
- response to LPS (Figures 5G-H).

395 Traffic of myeloid progenitors to regional LNs was recapitulated in mice receiving 396 intrafemoral adoptive transfer of GMP (Figures 51-J). In these mice, in vivo L-selectin blockade did not abrogate GMP migration to regional LN while sinusoidal-dependent B-lymphocyte 397 398 mobilization into regional LN was significantly impaired (Figures 5J-K), indicating that the 399 migration of BM myeloid progenitors, unlike B cells, into the regional lymphatic circulation is Lselectin independent and therefore unlikely to be mediated by LN high endothelial venules 400 (HEV) (Rosen, 2004). Altogether, these data strongly indicated that Ccl19/Ccr7 chemokine 401 402 signaling is required for the rapid migration of myeloid progenitors to LN upon LPS 403 administration and that Ccr7 signaling is required to prevent death within the first hours after LPS administration. Given the strong time association of these events, these data support a role 404 for the Ccr7-dependent early traffic of myeloid progenitors in the amelioration or delay of the 405 406 endotoxic shock induced by LPS.

407

408 Ccl19 is expressed and pre-stored in cDC2 and released upon activation of IKK/Snap23.

409 Chemokine secretion requires endosomal fusion with the membrane which can be detected by exposure of the phosphatidylserine (PS)-rich inner leaflet of the endosomes to the 410 external surface of the cell membrane, providing a venue to determine what cell types were 411 responsible for the secretion of Ccl19. We found an increase in the levels of PS residues on the 412 413 outer membrane leaflet of WT LN cDC2 (defined as CD11b⁺/CD11c⁺), but not in the CD11b⁻ /CD11c⁺ population which comprises cDC1 and plasmacytoid DC (Figure 6A). Interestingly, the 414 exposure of PS residues was abrogated in Traf6^{4/2} LN cDC (**Figure 6A**) indicating that Traf6 415 also mediates the process of vesicle secretion upon LPS stimulation. Having demonstrated that 416 417 LPS/Traf6 signaling is required for chemokine traffic/secretion in LN mature myeloid-lineage

418 cells, and NF-KB transcriptional activation is dispensable for LPS-dependent myeloid progenitor 419 migration, we hypothesized that Traf6 acts through non-NF-kB dependent IKK activity. To determine whether canonical LPS/TLR downstream effectors were involved in the process of 420 421 myeloid progenitor migration, we analyzed the chemotaxis of BM myeloid progenitors towards a 422 gradient generated by LN cells in the presence of LPS and specific inhibitors for interleukin 423 receptor associated kinase 1/4 (Irak1/4), ubiguitin-conjugating enzyme 13 (Ubc13), and IKKB 424 (Figure 6B). Increased myeloid progenitor migration was reversed by all three specific inhibitors (Figure 6B) indicating that the integrity of canonical signaling pathway upstream of NF-κB might 425 426 be required to attract myeloid progenitors from the BM to the LN. The Traf6/IKK dependent 427 rapid response to LPS strongly suggests that LPS induces secretion of Ccl19 through a mechanism of rapid release from pre-stored pools. The release of pre-formed cytokines in pre-428 pooled, stored late endosomes depends on IKK activity through the phosphorylation of 429 430 mediators of cell membrane fusion. SNAP23 is an essential component of the high affinity 431 receptor which is part of the general membrane fusion machinery and an important regulator of 432 transport vesicle docking and fusion (Karim et al., 2013; Suzuki and Verma, 2008), Phospho-433 SNAP23(Ser95) is significantly upregulated by LPS in LN cDC (Figure 6C). Each of the inhibitors for Irak1/4, Ubc13 and IKK abrogated the activation of SNAP23 (Figures 6C and 434 435 **S5H**). Altogether, this set of data indicates that the activation through Traf6/Irak1/4/Ubc13 436 induced by LPS activates vesicular fusion and vesicular cargo release of pre-formed Ccl19 accumulated in late endosomes of LN myeloid cells. Analysis of steady-state LN myeloid cell 437 438 populations identified a subpopulation of cDC but not pDC or macrophages, containing most of 439 the cytoplasmic expression of Ccl19. Further analysis of the subpopulations of LN cDC2 demonstrated that B220⁻/CD8⁻ cDC that expressed the endocytic receptor DEC-205 (CD205⁺) 440 441 and the mannose receptor signal regulatory protein α (SIRP α , CD172a⁺) distinctly stored high levels of cytosolic Ccl19 (Figures 6D and S6A) unlike other DC populations which expressed 442 low levels of Ccl19 (Figure S6B). These data indicate that a subpopulation of cDC2 stores 443 intracellular Ccl19 and is potentially able to self-regulate the migration of its own progenitors in 444 inflammation. 445

446 **DISCUSSION**

447

This study describes a previously unrecognized, rapid, emergent traffic of myeloid 448 449 progenitor cells from the BM via lymphatic vessels directly to lymphatic tissues that by-pass the 450 peripheral blood stream. Careful analysis of serial femoral sections has not unveiled the existence of a communication between lymphatic and blood vessels in BM further suggesting 451 452 the lack of communication between both circuits within the BM cavity and thus likely functional 453 regional independence of each circuit. Our data thus also supports the recently described existence of functional lymphatic vessels in the bone. High-resolution confocal and multiphoton 454 microscopy demonstrated the existence of Lyve1+ cells in which their transgenic reporter 455 456 illuminated upon exposure to high-dose LPS in vivo along with tiny projections of lymphatics 457 penetrating into the bone. Probably, bone processing and cleaning before fixation and decalcification may have deprived us (and other investigators) from a better identification of 458 459 notable, anatomically identifiable lymphatic vessels within the network of transcortical capillaries (Gruneboom et al., 2019). 460

461 Bone is a dynamic organ in constant remodeling. Upon inflammation for example, cytokines and microbial LPS are capable to initiate bone absorption by activating osteoclasts 462 (Hardy and Cooper, 2009; Nason et al., 2009). Systemic inflammation has been associated with 463 osteoclast activation and osteoblast thinning (Hardy and Cooper, 2009; Nason et al., 2009) and 464 465 bone lymphatic endothelial cells have been shown to arise rapidly from pre-existing regional lymphatics upon osteoclast activation (Hominick et al., 2018; Monroy et al., 2020). Osteoclast 466 467 activation and osteoblast thinning are likely to facilitate transcortical migration of cells and fluid 468 through existing transcortical vessels.

469 Our data showed that as early as 90 minutes after LPS administration, myeloid 470 progenitors to or are in closer proximity to the lymphatic endothelium in BM while 1.5 hours later 471 there is a ~70% reduction of myeloid progenitors within the BM and a marked increase of 472 myeloid progenitors in the LN tissue. This observation along with the need of a longer period of 473 time to detect an increase in the frequency of myeloid progenitors in peripheral blood suggests

474 that two temporally distinct waves of progenitors take place, a fast one to the lymphatic

475 circulation followed by a slower one into the blood stream.

476 In our study, by using transgenic animals, we demonstrated that the administration of a 477 single dose of LPS suffices to induce migration of GMP/MDP while no other types of progenitors or stem cells migrate to lymphatics in this first wave of egression before any significant 478 479 contribution from or to PB and replenish short-lived cDCs in murine acute model of inflammatory 480 signaling by LPS, and that therefore they may modulate the course of infectious diseases and other inflammatory conditions. This traffic is also likely to happen in homeostatic conditions as 481 482 previously shown (Waskow et al., 2008) while our analysis provides compelling evidence on its striking activation upon inflammation/LPS administration. 483

Our data support the migration of a distinctly immature progenitor population composed 484 485 of GMP/MDP with ability to generate cDC in LN upon traffic from BM to LN. This traffic of 486 myeloid progenitors from BM to LN can be recapitulated in mice receiving intrafemoral adoptive transfer of GMPs. These GMP/MDP tend to localize in the T-cell areas of LN. Cheong et al. 487 reported that migratory monocyte-derived cDC2 can also localize in T cell areas of the LN and 488 489 acquire an inflammatory phenotype DC-SIGN/CD209a⁺ (Cheong et al., 2010). No significant mobilization of M-CSF responding monocyte progenitors (CFU-M) can be found as early as 3 490 hours after LPS administration. Interestingly, the interference of this traffic by either blocking the 491 492 chemokine secretion by mature LysM-expressing myeloid cells, or by blocking the chemokine 493 receptor Ccr7 results in increased animal death, which strongly suggests that the traffic of progenitors resulting from Ccl19/Ccr7 signaling is not only destined to the differentiation into 494 495 cDC but also to a more immediate anti-inflammatory role as suppressors of the endotoxic shock effects. Ccr7⁺ GMP/MDP, but not other myeloid or lymphoid progenitors, egress BM. Such 496 497 egress follows differential tissue levels of Ccl19 resulting from activation of the secretion of the 498 pre-formed chemokine by LN LysM-expressing mature myeloid cells, specifically a subpopulation of cDC expressing CD205 and CD172a. This process seems to be independent 499 of Cxcl12 levels since no changes in Cxcl12 levels in LN, PB or BM were observed and this 500

501 effect seems to be exclusively dependent on activation of non-canonical Traft6/IKK activity

502 without need for transcriptional activation.

Schmid et al (Schmid et al., 2011) demonstrated that a population of common dendritic 503 504 progenitors (CDP), a non-GMP derived population of progenitors can also migrate from the BM 505 to lymphoid and non-lymphoid tissues in response to TLR agonists and generate both cDCs and 506 pDCs (pDCs). The type of migration though depended on combined downregulation of Cxcr4 507 and upregulation of Ccr7, which seem to imitate the mechanism of GMP migration. Interestingly, 508 Ccl21, which is expressed by lymphatic endothelial and stromal cells but not by myeloid cells 509 (Eberlein et al., 2010), does not induce any differential gradient of secretion between LN and 510 BM or blood suggesting that Ccl21 may not be a primary mediator of the myeloid progenitor migration from BM to LN upon LPS challenge, while the hematopoietic deficiency of Ccl19 511 suffices to completely abrogate the mobilization of myeloid progenitors to LN induced by LPS. 512

513 Our data support the existence of a steady-state LN population of cDC which coexpresses the maturation antigens CD205 and CD172a and store high levels of Ccl19 in their 514 515 cytoplasm. An interesting possibility is, as our data indicate, that upon bacterial antigen 516 challenge, differentiated myeloid cells of LN like cDCs, which respond to LPS by secreting chemokine-containing pre-formed exosomes, accelerate a positive feedback activation loop to 517 recruit cDC progenitors to the lymphatic tissue. cDC in LNs might thus act as sensors for the 518 presence of bacterial products and release Ccl19 within minutes. Individual DCs have a short 519 520 half-life (1.5-2.9 days)(Kamath et al., 2002) and DC precursors have a short half-life in blood 521 circulation (Breton et al., 2015). We posit that the migration of DC progenitors through the lymph 522 tissues provides a direct afferent communication between the LN mature cDC population responsible for the secretion of the chemokine Ccl19 and at the same time, allows the emergent 523 524 migration of functional cDC progenitors from the BM to replenish the repertoire of lymphatic 525 antigen presenting cells.

526 Finally, our data also support the key role of an alternative inflammatory signaling 527 pathway elicited by coordinated by Traf6/IKK responsible for SNAP23 phosphorylation and

528 Ccl19 secretion, before resulting in transcriptional regulation by their downstream effector NF-529 kB. Traf6 has been identified as a signaling molecule that can regulate splicing of downstream targets without affecting NF-kB in hematopoietic stem cells and progenitors (Fang et al., 2017). 530 Our data further identifies non-canonical signaling pathways elicited by Traf6 in differentiated 531 532 myeloid cells to modulate the inflammatory response affecting the circulatory dynamics of 533 hematopoietic progenitors. Traf6 dependent, cytosolic mediated inflammatory response allows a 534 fast response before inflammatory transcriptional and post-transcriptional signatures are 535 mounted. 536 In summary, we describe, upon inflammation, a rapid trafficking of cDC biased myeloid

progenitors from the BM, via lymphatic vessels, directly to lymphatic tissues that by-passes the blood stream. This GMP/MDP migration represents a mechanism for fast replenishment of cDCs in lymphatic tissues. Rapid replenishment of cDC-biased progenitors in LN may represent a major homeostatic function of this novel lymphatic circuit and may explain why the circulation of myeloid progenitors is conserved during the postnatal life.

542

544 MATERIAL AND METHODS

- 545
- 546 **Mice**

CD57BI/6 (CD45.2⁺) mice were used between 8-10 weeks of age and were purchased 547 from Jackson Laboratory, Bar Harbor, ME: Harlan Laboratories, Frederick, MD. Mx1Cre⁺:Traf6-548 549 floxed mice were generated by breeding Mx1-Cre transgenic mice(Mikkola et al., 2003) with biallelic TRAF6 floxed mice (kindly provided by Dr. Yongwon Choi, University of 550 551 Pennsylvania) (Kobayashi et al., 2003). Full chimeric mice were generated by non-competitive transplantation of *Mx1Cre^{Tg/+}*:WT or *Mx1Cre;Traf6^{flox/flox}* whole BM cells into lethally irradiated 552 B6.SJL^{Ptprca Pepcb/BoyJ} (CD45.1⁺) mice obtained from the CCHMC Animal Core. Traf6 was deleted 553 upon induced expression of Cre recombinase after 3-6 intraperitoneal injections (10 mg/Kg/b.w. 554 555 Poly(I:C); Amersham Pharmacia Biotech, Piscataway, NJ, USA) every other day at 6 weeks after transplantation. LysM-Cre;Traf6 floxed mice were generated by non-competitive 556 transplantation of LysMCre^{Tg/+};WT or LysMCre^{Tg/+}; Traf6^{flox/flox} whole BM cells into lethally 557 irradiated B6.SJL^{Ptprca Pepcb/BoyJ} (CD45.1⁺) mice obtained from the Division of Experimental 558 559 Hematology/Cancer Biology of Cincinnati Children's Hospital Research Foundation (CCHRF). 560 Lyve1-eGFP (Pham et al., 2010) and β-actin-eGFP (Okabe et al., 1997) and Cx3cr1-GFP(Jung et al., 2000) transgenic mice were purchased from Jackson Laboratories. C57BL/6 561 mice for circadian cycle analysis of CFU-C were maintained on a 14-hour light / 10-hour 562 563 darkness lighting schedule. This study was performed in strict accordance with the recommendations in the Guide for the Care and Use of Laboratory Animals of the National 564 565 Institutes of Health. All of the animals were handled according to approved institutional animal 566 care and use committee (IACUC) protocol #2019-0041 of Cincinnati Children's Hospital. 567

568 Human specimens

569 Lymphadenopathies from patients were obtained through Institutional Review Board-570 approved protocols of the Hospital Reina Sofia (Cordoba, Spain), donor informed consent and legal tutor approval in the case of patients younger than 18 years old. Diagnostic 571 lymphadenopathy biopsies from sixty-four consecutive patients from 2009 until 2013 were 572 573 analyzed in this study. The median age of patients was 34 years old (range: 3-89). Diagnosis and histological classification of the type of lymphadenopathy and tumors were based on 574 previously published criteria (Campo et al., 2011; Weiss and O'Malley, 2013). Anatomical 575 576 location of lymphadenopathies is described in Table 1. Specimens were blindly analyzed 577 through adjudication of unique identifiers.

578

579 LPS injection and samples collection

580 Mice received a single intraperitoneal injection of 30 mg per Kilo of E. coli LPS (Sigma-581 Aldrich, St Louis, MO) or PBS as vehicle control and were executed always at ZT4 or 4 hours after the initiation of light into the animal room. At different time points after PBS or LPS 582 administration, BM cells from femurs, tibias and pelvis were harvested by crushing in PBS 583 584 containing 2% of FBS and erythrocytes were lysed using a hypotonic buffer from BD 585 Biosciences. Blood was collected by retro-orbital bleeding or cardiac injection. Liver, kidney and thoracic duct cells were harvested by enzymatic digestion solution with collagenase II (1 mg/mL, 586 587 ThermoFisher Gibco, Waltham, MA) and dispase (5 mg/mL, Gibco, Life Technologies) in a shaking water bath at 37°C for 1h. Spleen cells were isolated by scraping with slides in sterile 588 PBS following red blood cell (RBC) lysis (Pharm Lyse[™]; BD Bioscience, San Jose, CA). 589 Extracted LN were derived from the cervical and axillary chains exclusively. 590

591

592

593 Myeloid progenitor counts assay in vitro

594 Cells from BM, lymph nodes, thoracic duct, blood, spleen, liver and kidneys were depleted of RBC by 2 minute-incubation in Pharm Lyse[™] (BD Biosciences, San Jose, CA), 595 washed, counted and plated in semisolid methylcellulose media (Methocult 3434; StemCell 596 Technology, Vancouver, Canada) and cultured in an incubator (37°C, 5% CO₂/>95% humidity) 597 598 and the number of CFU-C was scored on day 7 or 8 of culture using an inverted microscope. To examine the type of myeloid progenitors migrating into LN, we used base methylcellulose 599 medium (Methocult 3134; StemCell Technology, Vancouver, Canada) supplemented with 30% 600 601 FCS, 1% protease-free, deionized BSA (Roche), 100 mM b-mercaptoethanol, 100 IU/mL 602 penicillin, 0.1 mg/mL streptomycin andany of the following: for CFU-GM, rm-GM-CSF (100ng/mL, PeproTech Rocky hill NJ) for specific analysis of CFU-GM content, rm-M-CSF 603 (100ng/mL, PeproTech Rocky hill NJ) for specific analysis of CFU-M content or rh-G-CSF 604 (100ng/mL, Neupogen) for specific analysis of CFU-G content. 605

606

607 Long-term competitive repopulation assay

To analyze the long-term reconstitution capacity of HSC/Ps mobilized into LNs after LPS 608 609 administration at different time of periods, 4-5x10⁶ of erythrocyte-depleted CD45.2⁺ LN 610 suspension cells were prepared in sterile conditions and transplanted together with 2.5x10⁵ CD45.1⁺ BM competitor cells into lethally irradiated CD45.1⁺ recipient mice. In some 611 experiments, 10⁴ LN SP cells or 10³ BM SP cells from CD45.2⁺ mice were competitively 612 transplanted into CD45.1⁺ recipient mice. Competitive repopulating units (CRU) analysis was 613 performed by flow cytometry analysis (BD Biosciences) at different time points post-614 transplantation(Harrison, 1980). 615

616

617 Flow cytometry analysis and cell sorting.

618 For immunophenotype analysis of HSC/P populations by fluorescence-activated cell 619 sorter (FACS), erythrocyte-depleted BM cells were stained first for lineage markers with biotin-

620	labeled mouse lineage panel (BD Biosciences, Pharmingen) containing anti-CD3e (CD3 $_{\epsilon}$ chain),
621	anti-TER-119/Erythroid cells (Ly-76), anti-Gr1 (Ly6G and Ly-6C), anti-CD45R (B220), anti-
622	CD11b (integrin α chain, Mac1 α) followed of allophycocyanin and cyanine dye Cy7-(APC-Cy7)
623	conjugated streptavidin, allophycocyanin (APC)-conjugated anti-c-Kit (clon 2B8), R-
624	phycoerythrin and cyanine dye Cy7 (PECy7)-conjugated anti-Sca1 (clone D7), eFluor 450-
625	conjugated anti-CD34 (clone RAM34) (affymetrix eBioscience, San Diego CA), PerCP and
626	cyanine dye Cy5.5 (PerCP Cy5.5)-conjugated anti-Fcy-RII/III (clone 2.4G2) (BD Biosciences).
627	FACS sequential discrimination on a Lineage negative gated population was used to identified
628	LK myeloid progenitor subpopulations: Lin ⁻ ,c-Kit ⁺ Sca1 ⁻ CD34 ⁺ FcγRII/III ⁺ (granulocyte-
629	macrophage progenitors, GMP); Lin ⁻ ,c-Kit ⁺ Sca1 ⁻ CD34 ⁺ FcγRII/III ^{lo} (common myeloid progenitors,
630	CMP); Lin ⁻ cKit ⁺ Sca1 ⁻ CD34 ⁺ FcγRII/III ⁻ . LSK (Lin-Sca1+c-Kit-) subpopulations were
631	distinguished as Lin ⁻ ,c-Kit ⁻ Sca1 ⁺ CD34 ⁻ Flt3 ⁻ for LT-HSC Lin ⁻ ,c-Kit ⁻ Sca1 ⁺ CD34 ⁺ Flt3 ⁻ for ST-HSC
632	and Lin ⁻ ,c-Kit ⁻ Sca1 ⁺ CD34 ⁺ Flt3 ⁺ for multipotent progenitors (MPP). For chimera analysis in
633	repopulated animals, 20 μ L of red cell-depleted blood was stained with fluorescein
634	isothiocyanate (FITC)-conjugated anti-CD45.1 (clone A20), R-phycoerythrin and cyanine dye
635	Cy7 (PECy7)-conjugated anti-CD45.2 (clone 104), allophycocyanin (APC)-conjugated anti-
636	CD11b (clone M1/70), allophycocyanin and cyanine dye Cy7-(APC-Cy7)-conjugated anti-B220
637	(clone RA3-6B2), R-phycoerythrin (PE)-conjugated anti-CD3e (clone 145-2C11) and BD
638	Horizon™ V450-conjugated anti-Gr1 (clone RB6-8C5), PerCPefluor [®] 710 anti-CD115 (clone
639	AFS98) and R-phycoerythrin conjugated anti-CD135 or anti-Flt3 (clone A2F0.1). All monoclonal
640	antibodies were purchased from BD, Pharmingen. Cell acquisition was performed by flow
641	cytometry (LSRFortessa I, BD Biosciences) equipped with FACSDIVA ^{m} software (BD,
642	Biosciences) for multiparameter analysis of the data. FACS sorting strategies were: CD45.1 ⁻
643	CD45.2 ⁺ CD3 $_{\epsilon}$ ⁺ B220 ⁻ CD11b ⁻ for LN-T cells, CD45.1 ⁻ CD45.2 ⁺ CD3 $_{\epsilon}$ ⁻ B220 ⁺ /CD11b ⁻ for LN-B cells
644	and CD45.1 ⁻ CD45.2 ⁺ CD3 ϵ ⁻ /B220 ⁻ /CD11b ⁺ for LN-myeloid cells in a FACSAria II cell sorter (BD
645	Biosciences). For BM and LN -side population (SP) cells analysis and sorting, 2x10 ⁶ cells/mL
646	were stained with Hoescht 3342 (5 μ g/mL) as described previously ¹⁵ . For intracellular analysis
647	of the phosphorylated state of SNAP23 protein, surface antigen-labeled cells were fixed with

648 Cytofix buffer (BD Biosciences) for 20 min and then permeabilized using Cytofix/Cytoperm 649 buffer (BD Bioscience) for 20 minutes. After washing, cells were stained intracellularly using a rabbit non-conjugated monoclonal anti-phospho-SNAP23(Ser⁹⁵)(Karim et al., 2013) for 40 650 minutes in Perm/Wash Buffer 1x (BD Bioscience) with 0.5% of rabbit serum. Cells were then 651 652 incubated with a secondary Alexa Fluor® 488-conjugated (ThermoFisher-Invitrogen) goat antirabbit antibody for 40 minutes in Perm/Wash Buffer 1x with 0.5% of goat serum. All incubations 653 after cell stimulation were done on ice and in darkness. Single cell analysis was performed by 654 655 flow cytometry and the histogram-overlay graphed (LSRFortessa I; FlowJo xV0.7 software; BD 656 Biosciences). The mean fluorescence intensity (MFI) ratio was calculated as the ratio of the fluorescence intensities of LPS-stimulated to PBS-stimulated (control). 657

658

659 Annexin-V binding

LN suspension cells from Mx1Cre; WT and Mx1Cre; Traf6^{Δ/Δ} mice were obtained to 660 performed LPS stimulation. 10⁶ cells were plated into 24-well-plates and treated with PBS or 661 LPS for 1 hour. After 15 minutes labelling with surface antibodies against CD45.2 (Clone 104), 662 663 CD11c (clone HL3), CD11b (Clone M1/70) and B220 (clone RA3-6B2) the samples were washed twice and then stained for annexin-V for 15 minutes and in darkness. All antibodies we 664 purchased from BD Biosciences - Pharmingen. Single cell analysis was performed using flow 665 cytometry and the histogram-overlay graphed (LSRFortessa I; FlowJo xV0.7 software; BD 666 Biosciences). The MFI ratio between LPS MFI and PBS MFI was calculated. 667

668

669

670 Homing and seeding assays

For homing assays, $2x10^6$ of Lin⁻ cells, previously depleted by immunomagnetic selection (Lineage Cell Depletion kit, Miltenyi Biotec, Auburn CA), were stained by 1,1[']-dioctadecyl-3,3,3['],3', tetramethylindocarbocyanine perchlorate;CILC18(3) (5 μ M/mL Dil, ThermoFisher-

674	Invitrogen) and adoptively transferred intravenously into non-myeloablated Lyve1-GFP+ mice.
675	Seventeen hours later, one single LPS dose (3mg/mL) or vehicle control (PBS) was
676	administered intraperitoneally. 3 and 6 hours later (ZT7 or ZT10) mice were euthanized with
677	pentobarbital (60-80 mg/Kg) and the whole body was fixed using a freshly made solution of PBS
678	plus 2% of paraformaldehyde (PFA) and 0.05% of glutaraldehyde infused by perfusion pump
679	through left ventricle of the animal. 15-20 minutes later the BM cells and LN organs were
680	harvested and the percentage of labeled Lin ⁻ cells which had homed into BM was determined by
681	FACS analysis. The homing calculation was done as previously reported(Boggs, 1984).

682

683 Microscopy

Fixed LN organs were permeabilized for 15 minutes with PBS containing 0.2% of Triton X-100. 684 685 To detect GFP on the lymphatic endothelium, LN were incubated overnight with a primary antibody anti-GFP+ (ThermoFisher-Invitrogen). LN were scanned by confocal microscopy 686 (Nikon A1R GaAsP) through multidimensional acquisition to construct 3D representations of the 687 688 whole organ at 10x magnification. The merged images of GFP/Dil or DAPI/Dil are presented 689 and the total cell number of labeled Lin⁻ cells was counted manually. Finally, harvested femurs 690 were decalcified for 14 days with 10% of EDTA (Sigma-Aldrich St Louis, MO) in PBS and 691 embedded in paraffin. Longitudinal section of bone were cut 4-um thickness and then were des-692 paraffinized and broke the protein cross-link before stain by antigen retrieval treatment with citrate buffer pH 6 (Cancelas et al., 2005). Then bone sections were permeabilized with 0.2% of 693 Triton X-100 for 15 min and blocked with 5% of BSA for 1h. Slides were stained with primary 694 695 antibodies anti-GFP (chicken polyclonal, Abcam Inc. Cambridge MA) and rat anti-mouse 696 panendothelial cell antigen (clone, MECA-32, BD Pharmingen) at 4°C overnight. Then we stained with secondary antibodies; goat anti-rat Alexa Fluor-488 and goat anti-chicken Alexa 697 698 Fluor-568, all from Invitrogen at 1:1000v/v concentration for 1h at room temperature. Blood and

699 lymphatic vessels were scanned by confocal microscopy (Nikon A1R GaAsP) through

700 multidimensional acquisition to construct 3D representation.

701 To further characterized lymphatic system in bone tissue and BM cavity and to image the close 702 proximity of homed Lin⁻/Dil⁺ to lymphatic vessels into Lyve1-eGFP⁺ mice, we utilized multiphoton intravital microscopy (IVM) as previously described (Gonzalez-Nieto et al., 2012; Kohler 703 704 et al., 2009). After LPS/PBS injections long bones were harvested and muscle were carefully 705 cleaned. Further, bone tissues were cautiously trimmed with an electric drill (Dremel) to get better excess of the BM cavity for imaging by leaving a very thin (~30-40 μ m) layer of bone 706 707 tissue. Bones were mounted in 2% low melting agarose to minimize movements during imaging 708 and covered with PBS. Multi-photon microscopy on the long bones (femur and tibia) was 709 subsequently performed using a Nikon A1R Multiphoton Upright Confocal Microscope equipped 710 with Coherent Chameleon II TiSapphire IR laser, tunable from 700 to 1000 nm and signal was detected by low-noise Hamamatsu photomultiplier (PMT) tubes. Bone tissue was identified as 711 712 second-harmonic (SHG) signal (PMT). Bones were images in PBS using a 25X Apo 1.1 NA 713 LWD water Immersion objective and NIS image software. For Initial standardization, bones were scanned at wavelength of 800, 850, 900 -nm detecting GFP (530 nm) and Dii red (580 nm). For 714 imaging, a 500 \times 500-µm area was scanned in ~35 steps of 4 µm down to 120-150 µm depth 715 716 using an illumination wavelength of 800 nm detecting SHG signal (480 nm), green (530 nm) and 717 red (580 nm) fluorescence. Control C57BL/6 mice were used as a negative control for Lyve-1 718 GFP mice to detect specific signal for GFP-lymphatic system in bone tissue and bone marrow cavity. Lymphatic vessels were well detected in the bone tissue using Lyve-1 GFP mice with Dil 719 720 labeled Lin⁻ cells in the BM cavity. For quantification of proximity of Lin⁻/Dil⁺ with Lymphatic 721 system, Imaris software was used to measure distance between Dil labeled cells and GFP 722 positive lymphatic vessels using 3D images.

723

724 Analysis of L-selectin dependence of femoral GMP/MDP migration to regional LN

725 C57BI6 mice received single intraperitoneal injections of MEL14 (CD62L) antibody (Biox-cell)

treatment, LDBM cells from ß-actin eGFP mice were injected intrafemorally. LPS (30mg/kg,

BW) was injected post 1hr. of interfemoral injections. Mice were sacrificed at 3 hours post-

administration and ipsilateral and contralateral regional and distant LNs (inguinal, popliteal,

730 axillary and cervical) were isolated for analysis. LN cells were stained GMP markers and anti-

731 CD19-PECy7 (Cat#552854, BD Biosciences) and analyzed by flow cytometry and quantified the

732 GFP⁺ GMP and B lymphocyte populations migrating to LN.

733

Femoral GFP⁺ progenitor migration in WT and Ccl19^{-/-} hematopoietic chimeras:

Hematopoietic chimeras of WT and Ccl19^{-/-} (Link et al., 2007) BM cells were generated by 735 transplantation into CD45.1+ mice, similarly to Mx1Cre;Traf6^{t/f} hematopoietic chimeras. Mice 736 737 were followed for 8 weeks and found to have >95% chimera of CD45.2+ cells in peripheral blood, After 8 weeks, femoral LDBM cells from donor congenic -actin transgenic, CD45.2+ mice 738 739 were injected (5x10⁵ per mouse) intrafemorally to both Wt and Ccl19 hematopoietic chimeric 740 mice. PBS or LPS (30mg/Kg. b.w.) were injected at 1 h post-intrafemoral injections and 741 sacrificed at 3 h post-administration of LPS. At that time, ipsilateral LN from inguinal and popliteal regions were isolated. Suspension of LN cells were counted and stained with specific 742 antibodies for GMP and MDP characterization, and the frequency of different GFP⁺ GMP and 743 744 MDP populations was analyzed by flow cytometry as mentioned above.

745

746 Chemotaxis/Migration assays

For non-cell autonomous effect analysis, $5x10^5$ of BM or LN nucleated cells from *Mx1Cre⁺;WT or Mx1Cre⁺;TRAF6*^{Δ/Δ} CD45.2⁺ were layered on bottom wells of 24-well transwell plate (Corning Inc., Lowell, MA) together with 100 ng/mL of LPS, and $1x10^5$ WT CD45.1⁺ LDBM cells were layered on upper chamber at 37°C, 5% CO₂. For cell autonomous effect analysis,

5x10⁵ of BM or LN nucleated cells from WT CD45.1⁺ mice were layered in the lower chamber 751 with 100 ng/mL of LPS, and $1 \times 10^5 M \times 1 Cre^{Tg/+}$; WT or $M \times 1 Cre^{Tg/+}$; Traf6^{\lambda} CD45.2⁺ LDBM cells 752 753 were layered in the upper chamber at 37°C, 5% CO₂. After 4 hours, cells were resuspended and 754 those adhered to the bottom layer were collected using an enzyme free cell dissociation buffer (Cell Dissociation Buffer, enzyme free, PBS, ThermoFisher-Gibco). Progenitor responses 755 toward migratory gradient were analyzed by flow cytometry analysis of LK cells. The percentage 756 757 of migration were calculated by dividing the number of LK in the outputs by the number of LK in the inputs and multiplied by 100. PBS was included as negative control. All assays were 758 759 performed in triplicate.

760

761 NFkB activity repression in myeloid cells

To analyze the NFkB-dependent or independent mechanism of myeloid progenitor 762 migration, BM Lin⁻ were transduced with pMSCVpuro-eGFP bicistronic retroviral vector 763 764 encoding the full length of IkBa mutant (super-repressor) in the presence of the recombinant 765 fragment of fibronectin, CH296 (Takara Bio Inc, Madison, WI) for 16 hours at 37°C. 24 hours later GFP⁺ cells were sorted and macrophages were generated (Chang et al., 2014). To 766 767 characterize the expanded population, R-phycoerythrin (PE)-conjugated anti-CD169 (clone 3D6.112), PerCP-efluor[®] 710-conjugated anti CD115 (clone AF598) (affymetrix eBioscience), 768 allophycocyanin and cyanine dye Cv7-(APC-Cv7) conjugated anti-CD11b. efluor[®] 450-769 conjugated anti-F4/80 (clone BM8) (affymetrix eBioscience), and Alexa Fluor[®] 647-conjugated 770 anti-CD68 (clone FA-11)(BD Biosciences) were used for FACS analysis. 50x10³ differentiated 771 772 and transduced macrophages with empty or IkBa super-repressor were layered on bottom wells of 24-well transwell plate in presence of 100 ng/mL of LPS and 1x10⁵ WT LDBM cells were 773 774 layered on upper chamber at 37°C, 5% CO₂. Four hours later migrated LK cells were determined by flow cytometry as described above. All assays were performed in triplicate. 775

776

777 Secretome and individual cytokine/chemokine analyses

778	BM, plasma and LN cells were isolated in PBS containing a protease inhibitor cocktail
779	(Roche Diagnostics, Chicago IL) and Ccl19/Ccl21 levels were determined by indirect sandwich
780	of enzyme-linked immunosorbent assay (ELISA) following manufacturer's instructions (R&D
781	Systems, Minneapolis, MN). Multi-analytic profiling beads using Milliplex® Multiplex mouse
782	cytokine/chemokine panel I kit (EMD Millipore, Billerica, MA) according to manufacturer's
783	instructions were used to analyze chemokines and cytokines profile into BM and LN tissues at
784	different time periods after LPS or PBS administration into WT mice.
785	
786	In vivo administration of anti-Ccr7 and anti-Ccl19
787	Monoclonal rat IgG2a antibody specific for Ccr7 (Clone 4B12) or polyclonal goat IgG
788	antibody for Ccl19 (AF880) and and control rat IgG2a or control goat purified IgG, were obtained
789	from R&D Systems. Fifty μ g of antibodies were injected twice into C56BL/6 mice within 15 hours
790	(first dose i.v. and the second dose i.p.)
791	
792	Small molecule inhibitors
793	The Irak1/4 Inhibitor I, ubiquitin-conjugating enzyme E2 N (UBE2N) inhibitor, Ubc13
794	inhibitor (Rhyasen et al., 2013) and IkB Kinase inhibitor (PS-1145 dihydrochloride) were
795	purchased from Sigma-Aldrich. LN cells from C57BL6 mice were treated with 10 μ M of IRAK-Inh,
796	0.2 μ M of Ubc13-Inh and 10 μ M of IKK-Inh for 45 minutes and compared with the vehicle
797	dimethylsulphoxide (DMSO) at 0.1% in PBS. Monensin (eBioscience) was used at 2 μ M.

798

799 Statistical analysis

800 Quantitative data is given as mean ± standard error of the mean (SEM) or standard deviation

801 (SD). Statistical comparisons were determined using an unpaired Student t-test, non-parametric

- 802 Mann-Whitney test, one-way or two-way Anova with Bonferroni corrections. A value of p< 0.05
- 803 was considered to be statistically significant.

805 **REFERENCES**

- Akira, S., Takeda, K., and Kaisho, T. (2001). Toll-like receptors: critical proteins linking innate and acquired immunity. Nat Immunol *2*, 675-680.
- Baldridge, M.T., King, K.Y., Boles, N.C., Weksberg, D.C., and Goodell, M.A. (2010). Quiescent
 haematopoietic stem cells are activated by IFN-gamma in response to chronic infection. Nature
 465, 793-797.
- 811 Bellet, M.M., Deriu, E., Liu, J.Z., Grimaldi, B., Blaschitz, C., Zeller, M., Edwards, R.A., Sahar, S.,
- Dandekar, S., Baldi, P., et al. (2013). Circadian clock regulates the host response to
- 813 Salmonella. Proc Natl Acad Sci U S A *110*, 9897-9902.
- 814 Beutler, B., and Rietschel, E.T. (2003). Innate immune sensing and its roots: the story of 815 endotoxin. Nat Rev Immunol *3*, 169-176.
- Boettcher, S., Ziegler, P., Schmid, M.A., Takizawa, H., van Rooijen, N., Kopf, M., Heikenwalder,
- M., and Manz, M.G. (2012). Cutting edge: LPS-induced emergency myelopoiesis depends on TLR4-expressing nonhematopoietic cells. J Immunol *188*, 5824-5828.
- Boggs, D.R. (1984). The total marrow mass of the mouse: a simplified method of measurement.
 Am J Hematol *16*, 277-286.
- 821 Bornhauser, M., Eger, L., Oelschlaegel, U., Auffermann-Gretzinger, S., Kiani, A., Schetelig, J.,
- 822 Illmer, T., Schaich, M., Corbeil, D., Thiede, C., et al. (2005). Rapid reconstitution of dendritic
- cells after allogeneic transplantation of CD133+ selected hematopoietic stem cells. Leukemia
 19, 161-165.
- Breton, G., Lee, J., Zhou, Y.J., Schreiber, J.J., Keler, T., Puhr, S., Anandasabapathy, N.,
- Schlesinger, S., Caskey, M., Liu, K., *et al.* (2015). Circulating precursors of human CD1c+ and CD141+ dendritic cells. J Exp Med *212*, 401-413.
- Brusnahan, S.K., McGuire, T.R., Jackson, J.D., Lane, J.T., Garvin, K.L., O'Kane, B.J., Berger,
- A.M., Tuljapurkar, S.R., Kessinger, M.A., and Sharp, J.G. (2010). Human blood and marrow
- side population stem cell and Stro-1 positive bone marrow stromal cell numbers decline with
 age, with an increase in quality of surviving stem cells: correlation with cytokines. Mechanisms
- 832 of ageing and development *131*, 718-722.
 - Campo, E., Swerdlow, S.H., Harris, N.L., Pileri, S., Stein, H., and Jaffe, E.S. (2011). The 2008
 WHO classification of lymphoid neoplasms and beyond: evolving concepts and practical
 applications. Blood *117*, 5019-5032.
 - 836 Cancelas, J.A., Lee, A.W., Prabhakar, R., Stringer, K.F., Zheng, Y., and Williams, D.A. (2005).
 - Rac GTPases differentially integrate signals regulating hematopoietic stem cell localization. Nat Med *11*, 886-891.
 - 839 Casanova-Acebes, M., Pitaval, C., Weiss, L.A., Nombela-Arrieta, C., Chevre, R., N, A.G.,
 - Kunisaki, Y., Zhang, D., van Rooijen, N., Silberstein, L.E., *et al.* (2013). Rhythmic Modulation of
 the Hematopoietic Niche through Neutrophil Clearance. Cell *153*, 1025-1035.
 - Challen, G.A., and Little, M.H. (2006). A side order of stem cells: the SP phenotype. Stem Cells
 24, 3-12.
 - Chang, K.H., Sengupta, A., Nayak, R.C., Duran, A., Lee, S.J., Pratt, R.G., Wellendorf, A.M., Hill,
 - S.E., Watkins, M., Gonzalez-Nieto, D., et al. (2014). p62 is required for stem cell/progenitor
 - retention through inhibition of IKK/NF-kappaB/Ccl4 signaling at the bone marrow macrophageosteoblast niche. Cell reports *9*, 2084-2097.
 - 848 Cheong, C., Matos, I., Choi, J.H., Dandamudi, D.B., Shrestha, E., Longhi, M.P., Jeffrey, K.L.,
 - Anthony, R.M., Kluger, C., Nchinda, G., et al. (2010). Microbial stimulation fully differentiates
 - 850 monocytes to DC-SIGN/CD209(+) dendritic cells for immune T cell areas. Cell 143, 416-429.

- Clausen, B.E., Burkhardt, C., Reith, W., Renkawitz, R., and Forster, I. (1999). Conditional gene targeting in macrophages and granulocytes using LysMcre mice. Transgenic Res *8*, 265-277.
- Cline, M.J., and Golde, D.W. (1977). Mobilization of hematopoietic stem cells (CFU-C) into the peripheral blood of man by endotoxin. Exp Hematol *5*, 186-190.
- Cross, M., Mangelsdorf, I., Wedel, A., and Renkawitz, R. (1988). Mouse lysozyme M gene:
 isolation, characterization, and expression studies. Proc Natl Acad Sci U S A *85*, 6232-6236.
- Esplin, B.L., Shimazu, T., Welner, R.S., Garrett, K.P., Nie, L., Zhang, Q., Humphrey, M.B.,
 Yang, Q., Borghesi, L.A., and Kincade, P.W. (2011). Chronic exposure to a TLR ligand injures
 hematopoietic stem cells. J Immunol *186*, 5367-5375.
- 860 Essers, M.A., Offner, S., Blanco-Bose, W.E., Waibler, Z., Kalinke, U., Duchosal, M.A., and
- Trumpp, A. (2009). IFNalpha activates dormant haematopoietic stem cells in vivo. Nature *458*, 904-908.
- Fang, J., Bolanos, L.C., Choi, K., Liu, X., Christie, S., Akunuru, S., Kumar, R., Wang, D., Chen,
 X., Greis, K.D., *et al.* (2017). Ubiguitination of hnRNPA1 by TRAF6 links chronic innate immune
- signaling with myelodysplasia. Nat Immunol *18*, 236-245.
- Fogg, D.K., Sibon, C., Miled, C., Jung, S., Aucouturier, P., Littman, D.R., Cumano, A., and
 Geissmann, F. (2006). A clonogenic bone marrow progenitor specific for macrophages and
 dendritic cells. Science *311*, 83-87.
- Forster, R., Davalos-Misslitz, A.C., and Rot, A. (2008). CCR7 and its ligands: balancing immunity and tolerance. Nat Rev Immunol *8*, 362-371.
- Forster, R., Schubel, A., Breitfeld, D., Kremmer, E., Renner-Muller, I., Wolf, E., and Lipp, M.
- 872 (1999). CCR7 coordinates the primary immune response by establishing functional
- 873 microenvironments in secondary lymphoid organs. Cell 99, 23-33.
- 6474 Geissmann, F., Jung, S., and Littman, D.R. (2003). Blood monocytes consist of two principal subsets with distinct migratory properties. Immunity *19*, 71-82.
- 876 Gonzalez-Nieto, D., Li, L., Kohler, A., Ghiaur, G., Ishikawa, E., Sengupta, A., Madhu, M., Arnett,
- J.L., Santho, R.A., Dunn, S.K., et al. (2012). Connexin-43 in the osteogenic BM niche regulates
- its cellular composition and the bidirectional traffic of hematopoietic stem cells and progenitors.
- 879 Blood *119*, 5144-5154.
- Goodell, M.A., Brose, K., Paradis, G., Conner, A.S., and Mulligan, R.C. (1996). Isolation and
- functional properties of murine hematopoietic stem cells that are replicating in vivo. J Exp Med
 183, 1797-1806.
- Gorgens, A., Radtke, S., Mollmann, M., Cross, M., Durig, J., Horn, P.A., and Giebel, B. (2013).
- 884 Revision of the human hematopoietic tree: granulocyte subtypes derive from distinct 885 hematopoietic lineages. Cell reports *3*, 1539-1552.
- Greenbaum, A., Hsu, Y.M., Day, R.B., Schuettpelz, L.G., Christopher, M.J., Borgerding, J.N.,
 Nagasawa, T., and Link, D.C. (2013). CXCL12 in early mesenchymal progenitors is required for
 haematopoietic stem-cell maintenance. Nature *495*, 227-230.
- Gruneboom, A., Hawwari, I., Weidner, D., Culemann, S., Muller, S., Henneberg, S., Brenzel, A.,
- 890 Merz, S., Bornemann, L., Zec, K., et al. (2019). A network of trans-cortical capillaries as
- mainstay for blood circulation in long bones. Nat Metab *1*, 236-250.
- Hardy, R., and Cooper, M.S. (2009). Bone loss in inflammatory disorders. J Endocrinol 201,
 309-320.
- Harrison, D.E. (1980). Competitive repopulation: a new assay for long-term stem cell functional capacity. Blood *55*, 77-81.

- Hominick, D., Silva, A., Khurana, N., Liu, Y., Dechow, P.C., Feng, J.Q., Pytowski, B., Rutkowski,
- J.M., Alitalo, K., and Dellinger, M.T. (2018). VEGF-C promotes the development of lymphatics in bone and bone loss. Elife 7.
- Jung, S., Aliberti, J., Graemmel, P., Sunshine, M.J., Kreutzberg, G.W., Sher, A., and Littman,
- D.R. (2000). Analysis of fractalkine receptor CX(3)CR1 function by targeted deletion and green
 fluorescent protein reporter gene insertion. Mol Cell Biol 20, 4106-4114.
- Kaisho, T., and Akira, S. (2001). Dendritic-cell function in Toll-like receptor- and MyD88 knockout mice. Trends Immunol 22, 78-83.
- Kamath, A.T., Henri, S., Battye, F., Tough, D.F., and Shortman, K. (2002). Developmental kinetics and lifespan of dendritic cells in mouse lymphoid organs. Blood *100*, 1734-1741.
- Karim, Z.A., Zhang, J., Banerjee, M., Chicka, M.C., Al Hawas, R., Hamilton, T.R., Roche, P.A.,
 and Whiteheart, S.W. (2013). IkappaB kinase phosphorylation of SNAP-23 controls platelet
 secretion. Blood *121*, 4567-4574.
- Karin, M., and Greten, F.R. (2005). NF-kappaB: linking inflammation and immunity to cancer
 development and progression. Nat Rev Immunol *5*, 749-759.
- Kawai, T., and Akira, S. (2006). TLR signaling. Cell Death Differ *13*, 816-825.
- Kim, C.H., Pelus, L.M., White, J.R., and Broxmeyer, H.E. (1998). Macrophage-inflammatory
- 913 protein-3 beta/EBI1-ligand chemokine/CK beta-11, a CC chemokine, is a chemoattractant with a
- specificity for macrophage progenitors among myeloid progenitor cells. J Immunol *161*, 2580 2585.
- 916 Kobayashi, T., Walsh, P.T., Walsh, M.C., Speirs, K.M., Chiffoleau, E., King, C.G., Hancock,
- 917 W.W., Caamano, J.H., Hunter, C.A., Scott, P., *et al.* (2003). TRAF6 is a critical factor for 918 dendritic cell maturation and development. Immunity *19*, 353-363.
- Kohler, A., Schmithorst, V., Filippi, M.D., Ryan, M.A., Daria, D., Gunzer, M., and Geiger, H.
- 920 (2009). Altered cellular dynamics and endosteal location of aged early hematopoietic progenitor 921 cells revealed by time-lapse intravital imaging in long bones. Blood *114*, 290-298.
- Kwak, H.J., Liu, P., Bajrami, B., Xu, Y., Park, S.Y., Nombela-Arrieta, C., Mondal, S., Sun, Y.,
 Zhu, H., Chai, L., *et al.* (2015). Myeloid cell-derived reactive oxygen species externally regulate
 the proliferation of myeloid progenitors in emergency granulopoiesis. Immunity *42*, 159-171.
- 925 Legler, D.F., Loetscher, M., Roos, R.S., Clark-Lewis, I., Baggiolini, M., and Moser, B. (1998). B
- 926 cell-attracting chemokine 1, a human CXC chemokine expressed in lymphoid tissues,
 927 selectively attracts B lymphocytes via BLR1/CXCR5. J Exp Med *187*, 655-660.
- Link, A., Vogt, T.K., Favre, S., Britschgi, M.R., Acha-Orbea, H., Hinz, B., Cyster, J.G., and
 Luther, S.A. (2007). Fibroblastic reticular cells in lymph nodes regulate the homeostasis of naive
 T cells. Nat Immunol *8*, 1255-1265.
- Luther, S.A., Tang, H.L., Hyman, P.L., Farr, A.G., and Cyster, J.G. (2000). Coexpression of the
 chemokines ELC and SLC by T zone stromal cells and deletion of the ELC gene in the plt/plt
 mouse. Proc Natl Acad Sci U S A *97*, 12694-12699.
- Martin, G.S., Mannino, D.M., Eaton, S., and Moss, M. (2003). The epidemiology of sepsis in the United States from 1979 through 2000. N Engl J Med *348*, 1546-1554.
- Massberg, S., Schaerli, P., Knezevic-Maramica, I., Kollnberger, M., Tubo, N., Moseman, E.A.,
 Huff, I.V., Junt, T., Wagers, A.J., Mazo, I.B., *et al.* (2007). Immunosurveillance by hematopoietic
- progenitor cells trafficking through blood, lymph, and peripheral tissues. Cell *131*, 994-1008.
- Matsuzaki, Y., Kinjo, K., Mulligan, R.C., and Okano, H. (2004). Unexpectedly efficient homing capacity of purified murine hematopoietic stem cells. Immunity *20*, 87-93.
- Mendez-Ferrer, S., Lucas, D., Battista, M., and Frenette, P.S. (2008). Haematopoietic stem cell release is regulated by circadian oscillations. Nature *452*, 442-447.

- 943 Mendez-Ferrer, S., Michurina, T.V., Ferraro, F., Mazloom, A.R., Macarthur, B.D., Lira, S.A.,
- 944 Scadden, D.T., Ma'ayan, A., Enikolopov, G.N., and Frenette, P.S. (2010). Mesenchymal and
- haematopoietic stem cells form a unique bone marrow niche. Nature *466*, 829-834.
- Mikkola, H.K., Klintman, J., Yang, H., Hock, H., Schlaeger, T.M., Fujiwara, Y., and Orkin, S.H.
 (2003). Haematopoietic stem cells retain long-term repopulating activity and multipotency in the
 absence of stem-cell leukaemia SCL/tal-1 gene. Nature *421*, 547-551.
- Monroy, M., McCarter, A.L., Hominick, D., Cassidy, N., and Dellinger, M.T. (2020). Lymphatics in bone arise from pre-existing lymphatics. Development *147*.
- 951 Mori, S., Nakano, H., Aritomi, K., Wang, C.R., Gunn, M.D., and Kakiuchi, T. (2001). Mice lacking
- expression of the chemokines CCL21-ser and CCL19 (plt mice) demonstrate delayed but
 enhanced T cell immune responses. J Exp Med *193*, 207-218.
- Nagai, Y., Garrett, K.P., Ohta, S., Bahrun, U., Kouro, T., Akira, S., Takatsu, K., and Kincade,
 P.W. (2006). Toll-like receptors on hematopoietic progenitor cells stimulate innate immune
 system replenishment. Immunity *24*, 801-812.
- Nason, R., Lee, D.H., Jung, J.Y., and Chole, R.A. (2009). Radiographic and micro-computed
 tomographic imaging of lipopolysaccharide-mediated bone resorption. Ann Otol Rhinol Laryngol
 118, 391-396.
- 960 O'Keeffe, M., Fancke, B., and Hochrein, H. (2010). The generation of plasmacytoid and 961 conventional dendritic cells with M-CSF. Methods in molecular biology *595*, 187-193.
- Okabe, M., Ikawa, M., Kominami, K., Nakanishi, T., and Nishimune, Y. (1997). 'Green mice' as a source of ubiquitous green cells. FEBS letters *407*, 313-319.
- 964 Pham, T.H., Baluk, P., Xu, Y., Grigorova, I., Bankovich, A.J., Pappu, R., Coughlin, S.R.,
- McDonald, D.M., Schwab, S.R., and Cyster, J.G. (2010). Lymphatic endothelial cell sphingosine
 kinase activity is required for lymphocyte egress and lymphatic patterning. J Exp Med 207, 17 27.
- Rhyasen, G.W., Bolanos, L., Fang, J., Jerez, A., Wunderlich, M., Rigolino, C., Mathews, L.,
 Ferrer, M., Southall, N., Guha, R., *et al.* (2013). Targeting IRAK1 as a therapeutic approach for
 myelodysplastic syndrome. Cancer Cell *24*, 90-104.
- Rosen, S.D. (2004). Ligands for L-selectin: homing, inflammation, and beyond. Annu Rev
 Immunol 22, 129-156.
- Saeki, H., Moore, A.M., Brown, M.J., and Hwang, S.T. (1999). Cutting edge: secondary
- 974 lymphoid-tissue chemokine (SLC) and CC chemokine receptor 7 (CCR7) participate in the
 975 emigration pathway of mature dendritic cells from the skin to regional lymph nodes. J Immunol
 976 162, 2472-2475.
- Sallusto, F., and Lanzavecchia, A. (2000). Understanding dendritic cell and T-lymphocyte traffic
 through the analysis of chemokine receptor expression. Immunol Rev *177*, 134-140.
- Schmid, M.A., Takizawa, H., Baumjohann, D.R., Saito, Y., and Manz, M.G. (2011). Bone
 marrow dendritic cell progenitors sense pathogens via Toll-like receptors and subsequently
- migrate to inflamed lymph nodes. Blood *118*, 4829-4840.
- Suzuki, K., and Verma, I.M. (2008). Phosphorylation of SNAP-23 by IkappaB kinase 2 regulates
 mast cell degranulation. Cell *134*, 485-495.
- Takeuchi, O., and Akira, S. (2010). Pattern recognition receptors and inflammation. Cell *140*, 805-820.
- Velders, G.A., van Os, R., Hagoort, H., Verzaal, P., Guiot, H.F., Lindley, I.J., Willemze, R.,
- 987 Opdenakker, G., and Fibbe, W.E. (2004). Reduced stem cell mobilization in mice receiving 988 antibiotic modulation of the intestinal flora: involvement of endotoxins as cofactors in
- 989 mobilization. Blood *103*, 340-346.

- Vos, O., Buurman, W.A., and Ploemacher, R.E. (1972). Mobilization of haemopoietic stem cells
- 991 (CFU) into the peripheral blood of the mouse; effects of endotoxin and other compounds. Cell
- 992 Tissue Kinet 5, 467-479.
- Vos, O., and Wilschut, I.J. (1979). Further studies on mobilization of CFUs. Cell Tissue Kinet *12*,
 257-267.
- 995 Waskow, C., Liu, K., Darrasse-Jeze, G., Guermonprez, P., Ginhoux, F., Merad, M., Shengelia,
- 996 T., Yao, K., and Nussenzweig, M. (2008). The receptor tyrosine kinase Flt3 is required for 997 dendritic cell development in peripheral lymphoid tissues. Nat Immunol *9*, 676-683.
- Weiss, L.M., and O'Malley, D. (2013). Benign lymphadenopathies. Modern pathology : an
- official journal of the United States and Canadian Academy of Pathology, Inc *26 Suppl 1*, S88-96.
- 1001 Weksberg, D.C., Chambers, S.M., Boles, N.C., and Goodell, M.A. (2008). CD150- side
- population cells represent a functionally distinct population of long-term hematopoietic stem
 cells. Blood *111*, 2444-2451.
- Wright, D.E., Wagers, A.J., Gulati, A.P., Johnson, F.L., and Weissman, I.L. (2001).
 Physiological migration of hematopoietic stem and progenitor cells. Science *294*, 1933-1936.
- Zhao, J.L., Ma, C., O'Connell, R.M., Mehta, A., DiLoreto, R., Heath, J.R., and Baltimore, D.
 (2014). Conversion of danger signals into cytokine signals by hematopoietic stem and
- (2014). Conversion of danger signals into cytokine signals by hematopoietic stem and
 progenitor cells for regulation of stress-induced hematopoiesis. Cell Stem Cell *14*, 445-459.
- 2009 Zhou, S., Schuetz, J.D., Bunting, K.D., Colapietro, A.M., Sampath, J., Morris, J.J., Lagutina, I.,
- 1010 Grosveld, G.C., Osawa, M., Nakauchi, H., et al. (2001). The ABC transporter Bcrp1/ABCG2 is
- 1011 expressed in a wide variety of stem cells and is a molecular determinant of the side-population
- 1012 phenotype. Nat Med 7, 1028-1034.
- 1013

1015 ACKNOWLEDGEMENTS

- 1016
- 1017 We want to thank Dr. Andre Olsson for flow cytometry analysis advice and Ms. Margaret
- 1018 O'Leary for editing manuscript. We also want to thank Dr. Andres Hidalgo (CNIC, Madrid, Spain
- 1019 and Yale University, New Haven, CT), Drs. Daniel Lucas, Leighton Grimes, Michael Jordan,
- 1020 Edith Jansen and Jizhou Zhang (Cincinnati Children's Hospital Medical Center) for helpful
- 1021 discussions on data interpretation and experimental approaches. This project has been funded
- 1022 by the Junta de Andalucía of Spain (J.S-L) and NIH R01 GM110628 and DK124115 grants
- 1023 (JAC). The authors declare they have no relevant conflicts of interest. We want to thank
- 1024 Francisco M. Gutierrez for human CFU-C pictures. We also want to thank Jeff Bailey and
- 1025 Victoria Summey for technical assistance and the Mouse and Research Flow Cytometry Core
- 1026 Facilities, both supported by the NIH/CEMH grant P30DK090971-01.

1028 FIGURE LEGENDS

Figure 1. Inflammation induces early mobilization of HSC/Ps to lymph organs in humansand mice.

1031	(A) Content of SP cells in human LN by flow cytometry. LN biopsies had been blindly
1032	identified histologically as lymphadenitis, subcategorized in follicular (FL, black circles n=21),
1033	granulomatous (GL, green circles N=7) and viral (VL, pink circles n=5) and lymphomas,
1034	subcategorized in Hodgkin's lymphoma (HL, blue circles n=12) or non-Hodgkin's lymphoma
1035	(NHL, orange circles n=19). (B) Strategy for LPS administration and collection of tissues (blood,
1036	kidneys, liver, spleen, BM, LN and TD) at specific times. LPS or vehicle control PBS was
1037	administered at the early rest phase into C57BI/6 (CD45.2 $^{+}$) mice and tissue specimens were
1038	collected before (ZT4), 1h (ZT5), 3 h (ZT7), 6 h (ZT10) or 12h (ZT16) later. (C-I). Myeloid
1039	colony-forming-cell unit (CFU-C) content in the collected tissues at different circadian cycle
1040	times. CFU-C contained in blood (C), kidneys (D) liver (E), spleen (F), BM (G), LN (H) and TD
1041	(I) in response to PBS (black circles) or LPS (blue squares) at different circadian cycle times
1042	(n=3-4 mice per time point and treatment). Results are shown as mean \pm SEM. *P< 0.05,
1043	**P<0.01.

1044

1045 Figure 2. Draining of BM-derived lineage negative cells into lymphaticstem.

1046 (A) Schema for adoptive transfer of BM-derived Lineage negative cells (Lin) labeled with 1,1'-dioctadecyl-3,3,3',3'-tetramethylindocarbocyanine perchlorate (Dil) dye into lymphatic 1047 endothelium reporter Lyve1-eGFP⁺ mice. By 16 hours after cell transplantation, LPS or PBS 1048 were administered into the Lyve1-eGFP⁺ mice at ZT4 (0h). BM and LN cells were analyzed at 1049 1050 ZT5.5 (1.5h), ZT7 (3h) and ZT10 (6h) for labeled Lin cells (Lin/Dil⁺). (B) Frequency of Lin/Dil⁺ 1051 homed to BM (solid bars) (mosaic bars) after PBS (black solid bar) or LPS (blue solid bar) 1052 administration at ZT7 (3h) and ZT10 (6h). N=3 mice per time point and group in two independent experiments. Graph represent mean \pm SEM. *P<0.05. **P<0.01. 1053

1054 (C) Representative 3D reconstruction images of the whole bone by two-photon microscopy

showing lymphatic vessels from Lyve1 surface marker (red), nuclei with DAPI (Blue) and cortical
bone with second harmonic signal (SHG, light blue). The scale bars, 100 μm.

1057 (D, i-iv) Intravital two-photon microscopy imaging (IVM) of long bones from Lyve1-eGFP mice showing lymphatic vessels (displayed in green) near to the surface of the bone (blue, detected 1058 by SHG signal) and homed Lin⁻/Dil⁺ cells (displayed in red). (i,iii) IVM of PBS specimen. (ii,iv) 1059 1060 IVM of LPS specimen. (E,F) Analysis and quantification of the distance of homed Lin⁻/Dil⁺ (red) cells to Lyve1-EGFP+ (green) cells after PBS/LPS administration at ZT5.5 (1.5h) analyzed by 1061 1062 Imaris 7.7.2 software. (G) Two-photon microscopy examples of images of longitudinal femoral sections stained with anti-Lyve1 antibody and DAPI, and analyzed for specific fluorescence 1063 1064 signal and SHG for cortical bone. (H-I) Representative of 3D reconstitution images of PBS- and 1065 LPS-treated LN tissues (H) and cross-sections of LPS-treated LN (I) analyzed by confocal 1066 microscopy showing the location of mobilized Lin /Dil⁺ cells (red; nucleus stained by DAPI in 1067 blue) in relation with Lyve-1+ cells (green; nucleus stained by DAPI in blue). The Z-stack 1068 dimensions of upper panels were: $X=1266.95\mu$ m, $Y=1266.95\mu$ m and $Z=344\mu$ m. Calibrate: $XY=2.47\mu m$ and $Z=4\mu m$. Resolution: 512 x 512 x 86. The Z-stack dimensions of lower panels 1069 were: X=1259.36μm, Y=1259.36μm and Z=132μm. Calibrate: XY=2.46μm and Z=4μm. 1070 1071 Resolution of images were: 512 x 512 x 86. (J) Absolute count of mobilized Lin/Dil⁺ cells 1072 counted within LN at ZT7 (3h, solid bars) and ZT10 (6h, mosaic bars) after PBS/LPS administration. N=4-14 lymph nodes analyzed per time point and graph represent mean ± SEM. 1073 1074 *P< 0.05, **P<0.01.

1075

1076 Figure 3. LN-mobilized GMP preferentially differentiate into dendritic cells.

1077 (A) Comparative quantification of the content of bipotent and unipotent myeloid progenitors in 1078 LN at ZT7 (3h) after PBS/LPS administration at ZT4 (0h). (B) Schema of isolation and transfer 1079 of BM-derived GMP from β -Actin-GFP reporter mice (CD45.2⁺) into C57Bl/6 (CD45.2⁺) mice

1080 ($2x10^5$ GFP⁺-GMP cells/mouse, n=3 mice per group). After BM homing (17h), mice were treated

1081 with single and low dose of LPS (5mg/Kg) at ZT4 (day1) and 7 days later BM and LN tissues 1082 were analyzed for GFP expression in myeloid populations by flow cytometry. (C-D) Graphs represent the percentage of GFP⁺-GMP differentiated to granulocytes (solid bars, 1083 Gr1⁺⁺CD11b⁺CD11c⁻), macrophages (left mosaic bars, Gr1^{dim}CD11b⁺CD11c^{neg}) and cDC (right 1084 1085 mosaic bars, Gr1⁻CD11b⁺ CD11c⁺) 7 days post-transferring after PBS/LPS administration by flow cytometry into LN (C) and BM (D). Values represent as mean ± SEM. **P<0.01. (E) FACS 1086 strategy for MDP content in BM and LN tissues from Cx3cr1^{gfp+} reporter mice (4-5 mice per 1087 group). Phenotypically, MDP are defined as lineage-negative with high expression of the 1088 1089 chemokine receptor Cx3cr1, c-fms (CD115) and Flt3 (P2), and intermediate expression of c-Kit. (F-G) Graphs show absolute numbers of MDP present in BM (F) and LN (G) 3 hour later (ZT7 1090 [3h]) after PBS (black circles) or LPS (blue squares) administration. Values represent mean ± 1091 SEM *P<0.05, **P<0.01. 1092

1093

Figure 4. Traf6 is key regulator for migration of BM-derived myeloid progenitors to lymph
 nodes in a non-cell autonomous manner.

1096 (A) Schema of full chimeric mice made by non-competitive transplantation of CD45.2⁺ Mx1Cre:WT and Mx1Cre:Traf6^{flox/flox} BM cells into lethally irradiated CD45.1⁺ B6.SJL^{Ptprca} 1097 Pep3b/BoyJ. 6 weeks later Traf6 gene were deleted by intraperitoneal injection of poly(I:C). 1 week 1098 1099 later we performed PBS/LPS injection early in the rest phase (ZT4 [0h]) and LN-contained 1100 myeloid progenitors at ZT7 (3h) was scored by CFU assay. (B) Absolute number of CFU-GM presents in LN from Mx1Cre;WT (solid bars) and $Mx1Cre;Traf6^{\Delta/\Delta}$ (orange bars) full chimeric 1101 1102 mice (n= 6-7 mice per group) after PBS (black and orange solid bars) or LPS (blue and mosaic 1103 bars) administration. Values are shown as mean ± SEM of two independent experiments with a minimum of 3 mice per group *P< 0.05, **P<0.01. (C-H) In vitro transwell migration assay for 1104 BM-derived LK cells. (C) Experimental design for migration of WT or Traf6^{Δ/Δ} low-density 1105 (LD)BM cells (CD45.2⁺) toward a WT microenvironment generated by BM (CD45.1⁺) in the 1106 presence of LPS for 4 hours. (D) Graph represents the percentage migrated LK from WT (blue 1107

1108	solid bar) or Traf6 ^{Δ/Δ} (orange mosaic bar) low-density BM (LDBM) cells to the bottom as
1109	depicted in C. (E). Experimental design for migration of WT LDBM cells (CD45.1 ⁺) toward a
1110	gradient generated by WT/Traf6 ^{Δ/Δ} (CD45.2 ⁺) BM or LN cells in the presence of LPS for 4 hours.
1111	(F) Graph represents the percentage of LDBM LK migrated to the BM bottom (solid bars) or LN
1112	bottom (mosaic bars) as schemed in E. (G) Experimental design for WT LDBM cells (CD45.1 $^{+}$)
1113	migration toward gradient generated by WT/Traf6 ^{Δ/Δ} LN-derived T cells (CD45.2 ⁺ /CD3e ⁺ /CD11b ⁻
1114	/B220 ⁻) or B cells (CD45.2 ⁺ /CD3e ⁻ CD11b ⁻ /B220 ⁺) or myeloid cells (CD45.2 ⁺ /CD3e ⁻
1115	/CD11b ⁺ /B220 ⁻) in the presence of LPS for 4 hour. (H) Graph represents the percentage of
1116	migrated LK LDBM to the WT LN bottom (blue mosaic bars) or Traf6 $^{\Delta/\Delta}$ LN bottom (orange
1117	mosaic bars) as schemed G. In all cases, LK cell migration was determined by CD45 allotype
1118	analysis using flow cytometry in triplicate. Values are presented as mean \pm SD. (I) Absolute
1119	number of CFU-GM presents in LN from LysM-Cre;WT (solid bars) and LysM-Cre;Traf6 ^{Δ/Δ}
1120	(mosaic bars) full chimeric mice after PBS/LPS administration at ZT7 (3h). A minimum of 4 mice
1121	per group were analyzed. Values are presented as mean \pm SD, *P<0.05. **P<0.01. (J) Graph
1122	represent cumulative survival of LysM-Cre;WT (blue line) and LysM-Cre;Traf6 ^{Δ/Δ} (orange line)
1123	after 10 mg/Kg of LPS. **P<0.01. (J) Survival curve after 30 mg/Kg of b.w.injection in LysM-
1124	<i>Cre;WT</i> (blue line) <i>or LysM-Cre;Traf6</i> ^{Δ/Δ} (orange line). **P<0.01.

1125

1126Figure 5. GMP cells drain into local Lymphatics and not blood circulation in early

1127 inflammation via Ccl19/Ccr7

(A) Graph represents soluble Ccl19 chemokine in femoral or LN extracellular fluid and PB
plasma after PBS (black lines) or LPS (blue lines) administration at different circadian cycle
times (ZT4.5 [0.5h], ZT5 [1h] and ZT7 [3h]). Values represent mean ± SEM of two independent
experiments in duplicate. (B) Strategy for *in vivo* neutralization of Ccr7 receptor or Ccl19 ligand
by in2jections of anti-Ccr7 antibody or anti-Ccl19 antibody (50 µg/dose, two doses) into C57Bl/6
mice. One day after the last dose of antibodies, PBS or LPS was administered at ZT4 (0h) and
the myeloid progenitors-circulating cells from the LN and PB were measured by CFU assay at

1135 ZT7 (3h). (C-D) Absolute number of progenitors present into LN from neutralized mice with anti-Ccl19/IgG (left graph) or anti-Ccr7/IgG2a (right graph) after PBS (black) or LPS (blue) 1136 administration as depicted in B (n=7-8 mice per group). Values represent mean ± SEM. *P<0.05 1137 **P<0.01. (E-F) Survival curves after 30 mg/Kg LPS of b.w. (F) and 10 mg/Kg LPS of b.w. or 1138 1139 PBS as control (E, dashed lines) into WT C57BL/6 mice pre-treated with anti-Ccr7 (red line) or 1140 IgG2a (blue line). *P<0.05. (G) Generation of hematopoietic chimeric Ccl19 expressing (WT) or 1141 not (Ccl19^{-/-}) mice and isolation of LNs after administration of PBS or LPS. (H) Colony forming unit content of LN from either WT or Ccl19^{-/-} hematopoietic chimeric animals treated with PBS or 1142 1143 LPS (***p≤0.001). (I) Experimental design to analyze L-selectin dependence of femoral GMP migration to regional (or distant) LN after LPS administration. (J-K) Percentages of GFP ⁺ cells 1144 1145 in LN after administration of an isotype control or anti-L-selectin antibodies. (J) Frequency of 1146 GFP ⁺GMP cells in regional LN after administration of LPS was not modified by L-selectin 1147 blockade in vivo. (J) Inhibition of the migration of GFP⁺ B-lymphocytes to regional LNs in mice pre-treated with anti-L-selectin antibody (**p≤0.01). In B and C, LN were collected at ZT7 or 3h 1148 after LPS. 1149

1150

Figure 6. In vivo analysis of Ccl19/Ccr7 axis during inflammation. Pharmacological regulation of LPS/TLR signaling pathway.

1153 (A) Annexin-V binding to membrane PS on LN myeloid populations from WT (left mosaic bars) and Traf6^{$\Delta\Delta$} (right mosaic bars) (n=4 mice per group) after PBS or LPS administration. LN 1154 1155 suspension cells were stained for myeloid surface markers including annexin-V and analyzed by 1156 flow cytometry. Values represent mean ± SEM. **P<0.01. (B) Transwell migration of LDBMderived LK cells toward gradient generated by pre-treated LN cells with DMSO (solid bars) as 1157 vehicle control and inhibitors (mosaic bars) against Irak1/4 (right lined), Ubc13 (left lined), and 1158 1159 IKK (white squares), and following TLR signaling pathway activation by PBS (black) or LPS 1160 (blue). (C) Analysis of SNAP23 phosphorylation (Ser95) in LN myeloid cells previously treated with DMSO (solid bar) as vehicle control, Irak1/4 (right lined mosaic bar), Ubc13 (left lined 1161

1162	mosaic bar) or IKK (white squares mosaic bar) inhibitors. Values represent two independent
1163	experiments as mean \pm SEM of two independent experiments performed in triplicate. *P<0.05,
1164	**P<0.01. (D) Graph shows intracellular Ccl19 in LN-derived myeloid cells from non-
1165	manipulated mice by flow cytometry. Values represent mean \pm SEM of three independent
1166	experiments, n=8-9. ****P<0.0001.
1167	

- 1168 Supplementary Figure Legends

1169 Figure S1. Clonogenic and long-term multilineage potential of human and murine HSC/P

in LN. (A) Representative flow cytometry dot plots of SP cells from human LN biopsies

diagnosed with lymphadenitis (left flow panel) and non-Hodgkin Lymphoma (NHL, right flow

1172 panel). SP cells form a tail cluster on the left side. (B) Graph represents the percentage of SP

1173 cells in human LN biopsies categorized according to their anatomical location. Supra-

1174 diafragmatic location (solid circles) included neck and axillary LN and infra-diafragmatic location

1175 (open circles) included mesenteric and inguinal LN. (C) Representative colony-forming units

1176 (CFU-C) micrographs in human LN diagnosed with follicular lymphadenitis. Scale bar: 100 μm.

(D) Clonogenic potential of lymphadenitis-derived SP cells (upper left; with magnification of a

1178 CFU-GM in outlined inset) and FACS analysis of LN SP-derived hematopoietic progenitors

1179 (upper right and bottom panels) maintained for 1 week in culture as previously described(19).

All SP-derived progenitors were positive for pan-leukocyte surface marker CD45 but had

1181 heterogenic expression for CD34 and CD133 surface markers. (E) Absolute neutrophil count in

1182 PB from C57BI/6 mice pre-treated with PBS (black circles) or LPS (blue circles) at different

1183 circadian cycle times. (F-G). Representative FACS profiles of murine BM HSC/P in response to

in vivo administration of PBS (left panels) or LPS (right panels) at specified ZT. (H-O) Time

1185 response in the BM content of LSK (H), LT-HSC (I), ST-HSC (J), MPP (K), GMPs (L), CMP (\M),

1186 MEP (N) and LK cells (O) in response to PBS (black lines) or LPS (blue lines). Values represent

1187 mean ± SD of a minimum of 4 mice per group. *P<0.05, **P<0.01, ***P<0.001.

1189 Figure S2. Myeloid progenitor migration to LN in response to LPS is independent of

1190 NFkB activation. (A) Schema for the competitive long-term reconstitution potential of LN cells 1191 (donor cells) from C57BI/6 (CD45.2⁺) mice treated with PBS/LPS and harvested at ZT7(3h), into lethallv irradiated CD45.1⁺ B6.SJL^{Ptprca Pep3b/BoyJ} recipient mice (n=3 mice per group). (B-E) 1192 1193 Competitive repopulating unit (CRU) assay of LN cells as assessed by flow cytometry of 1194 allotype CD45.2 expressing cells in transplanted mice followed for up to 16 weeks. (B) Overall CRU as gated on CD45.2⁺ cells in response to donor cells from mice pre-treated with PBS 1195 1196 (black line) or LPS (blue line).(C-E) Myeloid cell (C), T-cell (D) and B-cell (E) contributing CRU 1197 in response to donor cells from mice pre-treated with PBS (solid bar) or LPS (blue mosaic bar). 1198 (F) Representative example of FACS analysis for SP cells (upper dot plots) and SP-LSK 1199 potential (lower dot plots) from PBS- and LPS-treated LN or BM tissues at ZT7 (3h). Hoechst: Hoechst 33342 staining for blue (blue) and red (red) fluorescence emissions. (G-H) Donor-1200

1201 derived chimera of sorted LN-or BM-SP cells obtained from LPS-treated mice.

1202

Figure S3. Myeloid progenitor migration to LN in response to LPS is independent of NFκB activation.

(A) Flow cytometry analysis of GFP MDPs in bone marrow showing decreased MDPs upon LPS 1205 1206 treatment. (B) Flow cytometry analysis of migrated GFP MDPs in lymph node (per regional 1207 group) showing increased GFP⁺MDPs in Inguinal and Popliteal lymph nodes. (Black bar EGFP⁺ 1208 and Blue Bar EGFP⁻. (C) Representative PCR amplifications show Traf6 deleted in circulating cells in four *Mx1cre;Traf6^{flox/flox}* mice after poly(I:C) injections (10mg/Kg/2 days x 5 doses). (D) 1209 Schema for BM-derived macrophages and exogenous expression of IkBa mutant which is 1210 1211 resistant to proteasome degradation. BM Lin⁻ cells were transduced with Pmscv-puro-eGFP 1212 bicistronic retroviral vector encoding full length of IkBa mutant and GFP⁺ protein. EGFP⁺ Lin⁻ cells were sorted and differentiated in culture by M-CSF cytokine to macrophages. Green 1213 1214 fluorescent CD11b+-macrophages were layered on bottom chamber and stimulated them with

1215	LPS to generate myeloid chemotaxis gradient. (E) FACS strategy for migrated LK (Lin ⁻ /c-
1216	Kit ⁺ /Sca1 ⁻) cells contained in LDBM from upper chamber to the transduced macrophage bottom
1217	stimulated with LPS and LPS+monensin (LPS+Mon) for 4 hours as depicted in J. (F)
1218	Representative FACS dot plots demonstrating gating strategy to identify migrating GMP
1219	populations from the transwell migration assays. (G) Graph represents LK cell migration
1220	towards transduced macrophages in presence of LPS (solid bars) or LPS+Mon (mosaic bars).
1221	Values represent mean±SD of three mice and per triplicate. NS: not significant. *P<0.05
1222	***P<0.001.

1223

1224 Figure S4. Inflammation induces temporal changes in chemokine and cytokine

signatures in BM and LN. (A) Cxcl12 in femoral or LN extracellular fluid and plasma after

1226 PBS/LPS *in vivo* administration at ZT7 (3h). (B) Heat map showing cytokine profiling release

into the extracellular fluid of femora and LN in response to PBS/LPS at ZT5 (1h) and ZT7 (3h).

1228 (C-O). Graphs represent levels of relevant cytokines and chemokines associated with

migration/inflammatory response and released into LN extracellular fluid (black and green bars)

1230 or into femoral extracellular fluid (black and orange bars) after PBS/LPS administration into

1231 C57BI/6 mice at ZT5 (1h) and ZT7 (3h). (C-J) Extracellular LN levels of Gm-csf (C), G-csf (D),

1232 M-Csf (E), Mcp-1 (F), Ccl5 (G), Eotaxin/Ccl11 (H), IL-13 (I), IL-5 (J). (K-N) Extracellular BM

1233 levels of Ccl3 (K), Ccl4 (L), Tnf α (M) and IL-1 α (N). Values are mean ± SE of two mice per

treatment and experiment, pooled from two independent experiments *P<0.05, **P<0.01,

1235 ***P<0.001, ****P<0.0001.

1236

1237 Figure S5. Myeloid expression of Ccl19 ligand in LN and short-term differentiation of pre-

1238 treated GMPs. (A) Ccl21 in femoral or LN extracellular fluid and PB plasma after PBS (left

1239 lines) or LPS (right lines) administration at different circadian cycle times. (B) Ccl19 released

1240 into the supernatant from sorted WT and Traf6-deficient LN T⁺ cells, B⁺ cells and CD11b⁺

1241 myeloid cells after LPS stimulation *in vitro*. Values represent mean ± SEM of two independent

1242	experiments. **P<0.01, ***P<0.001. (C-D). Membrane Ccr7 expression on GMP at ZT5 (1h)
1243	after PBS/LPS administration into WT and Traf6 deficient mice shows significant differences
1244	between groups. (C) Representative overlap histograms of Ccr7 expression on GMP-WT cells
1245	(upper) and GMP-Traf6 ^{Δ/Δ} (lower) cells after PBS (red line) or LPS (blue line). (D) Schema of
1246	transfer of Ccr7+ EGFP+ BM cells from b-actin-EGFP+ transgenic animals to femurs of WT
1247	recipient mice and administered PBS or LPS. (E-F) Femoral content of Ccr7-expressing GMP
1248	cells in BM (E) and regional (inguinal and popliteal) LN (F). (G) MFI of Ccr7 on GMPs from WT
1249	and Traf6 deficient mice in presence of PBS (black and orange solid bars) or LPS (blue solid
1250	bar and orange mosaic bar). Values represent mean mean \pm SD of three mice. (H)
1251	Representative overlap histograms of phospho-SNAP23 (pSNAP23) into LN myeloid cells
1252	treated with DMSO (upper left), Irak1/4-inh (upper right), Ubc13-inh (lower left) and IKK-inh
1253	(lower right) and stimulated with PBS (red lines) or LPS (blue lines).
1254	

1255 Figure S6. Basal Ccl19 detection into LN populations.

- 1256 (A) Gating strategy to determine Ccl19 pre-stored into LN-residing myeloid cells basally. (B-C)
- 1257 Mean fluorescence intensity (MFI) quantification of pre-stored Ccl19 into LN-residing

1258 CD11b^{low}/CD11c⁺ cDC (B) and pDC (C) populations in basal conditions.

1259

1261 Supplementary Movies

1262

1263 Movie S1 caption

- 1264 Representative example of multi-photon microscopy processed with Imaris software of a femur
- 1265 from one Lyve1-EGFP mouse treated with PBS at 1 hour after administration (ZT5). Bone tissue
- is identified as second-harmonic (SHG) signal (blue). Imaris software was used to measure
- 1267 distance between Dil labeled cells and GFP positive lymphatic vessels using 3D images.

1268

1269 Movie S2 caption

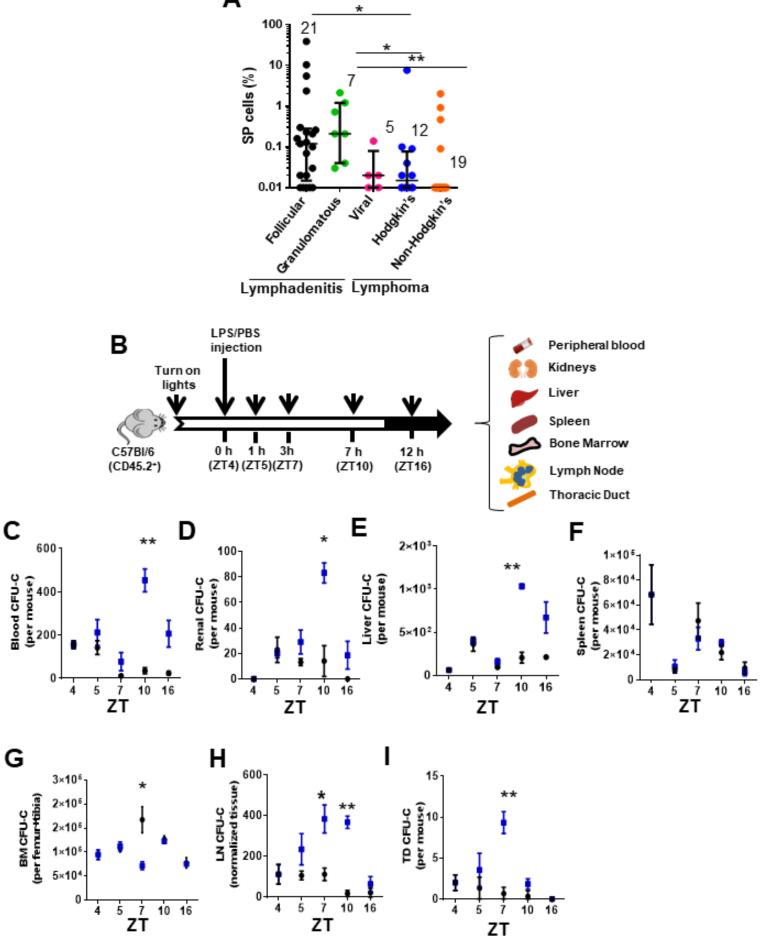
- 1270 Representative example of multi-photon microscopy processed with Imaris software of a femur
- 1271 from one Lyve1-EGFP mouse treated with LPS at 1 hour after administration (ZT5). Bone tissue
- 1272 is identified as second-harmonic (SHG) signal (blue). Imaris software was used to measure
- 1273 distance between Dil labeled cells and GFP positive lymphatic vessels using 3D images.

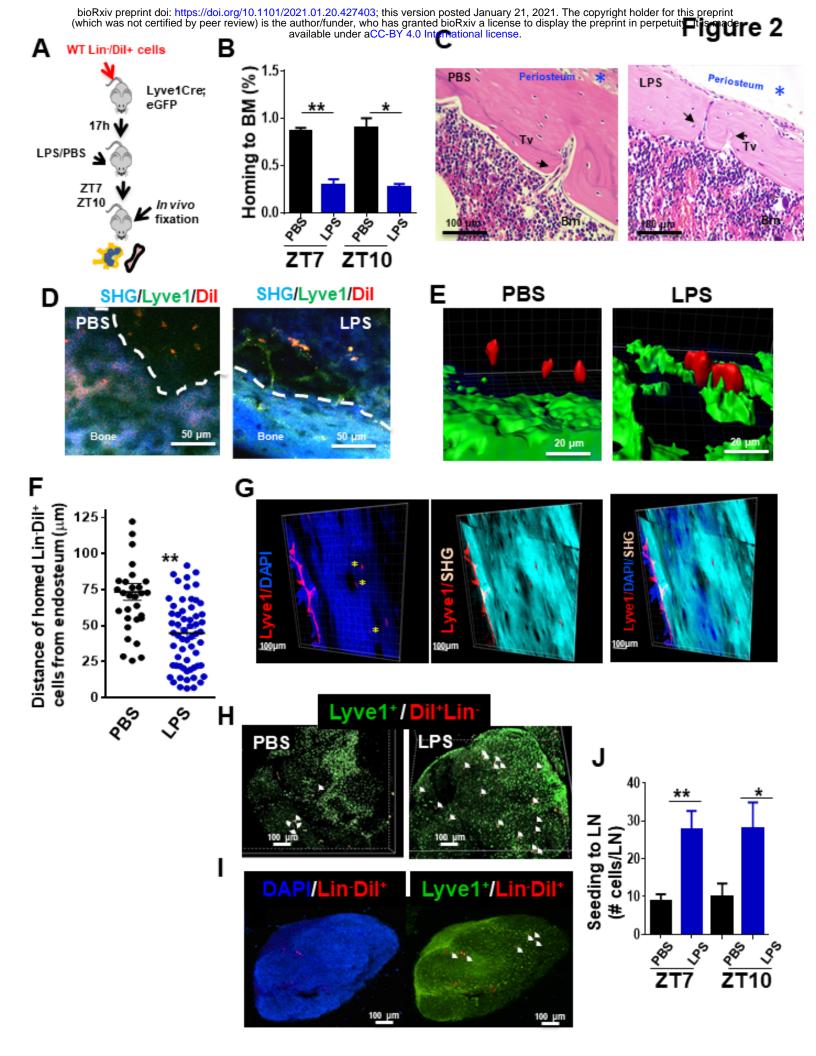
1274

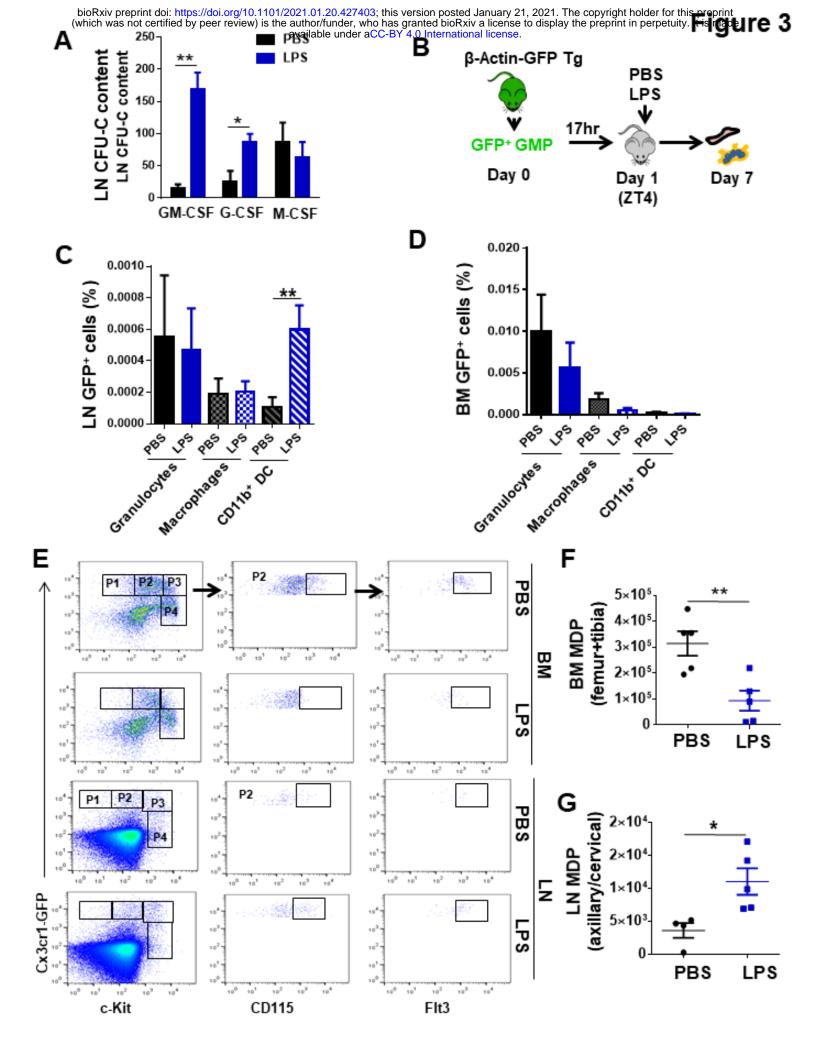
1275 Movie S3 caption

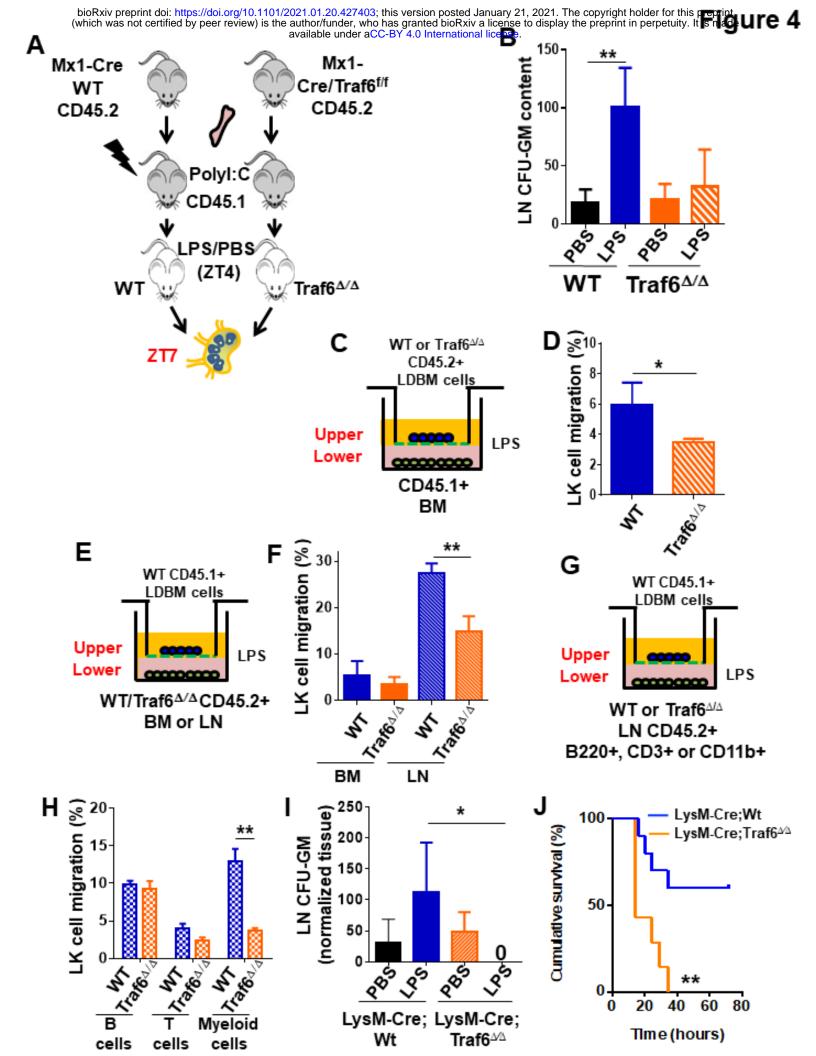
- 1276 Representative example of transcortical lymphatics discovered by staining with anti-Lyve1 (red)
- 1277 in wild-type C57BI/6 mice. Bone tissue is identified as second-harmonic (SHG) signal (blue).
- 1278 Green signal is autofluorescence.

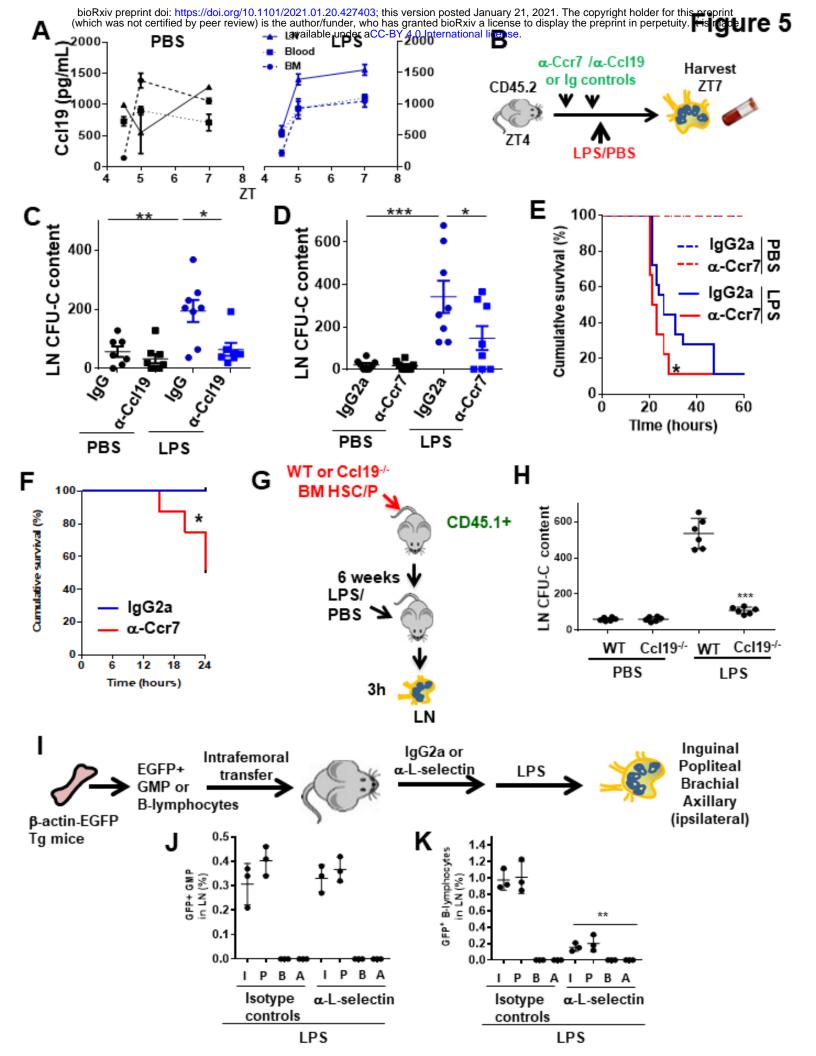
1279

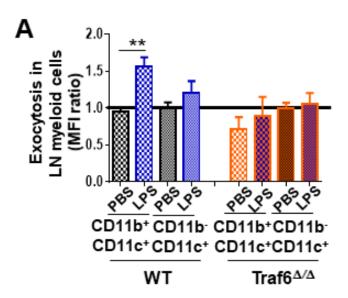


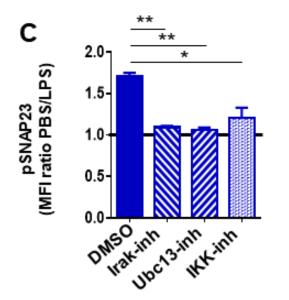


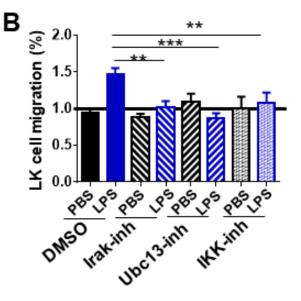


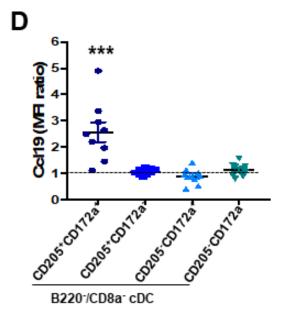


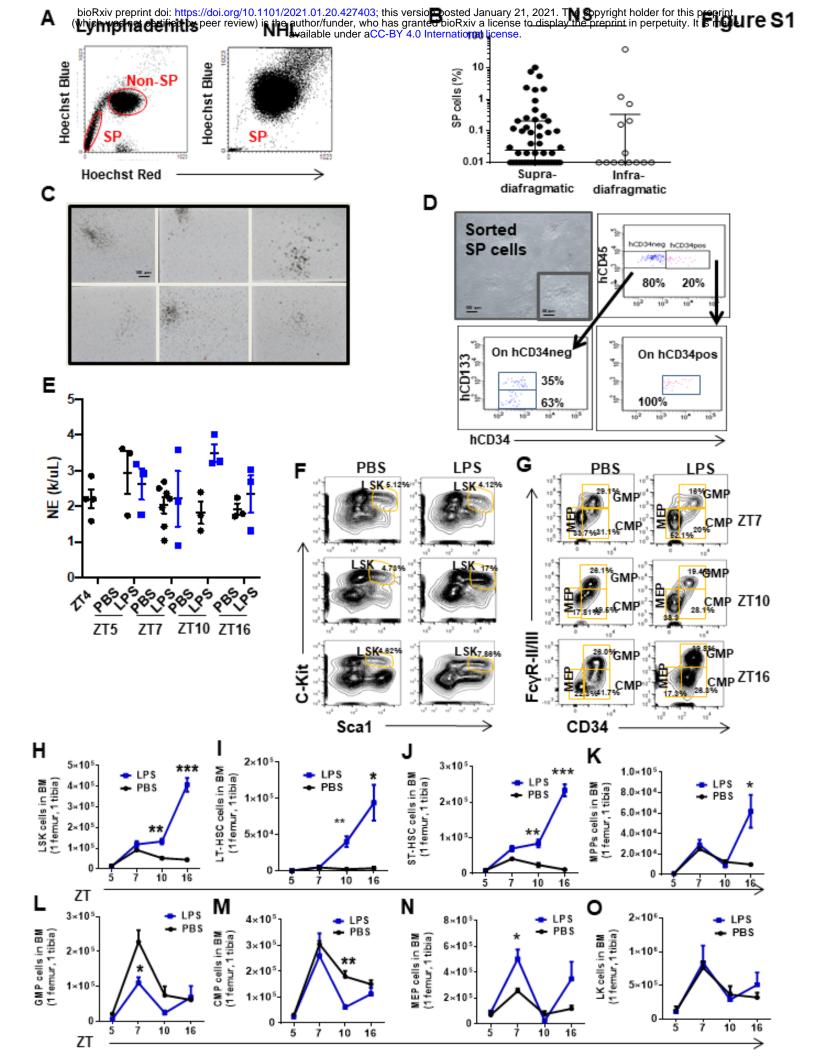


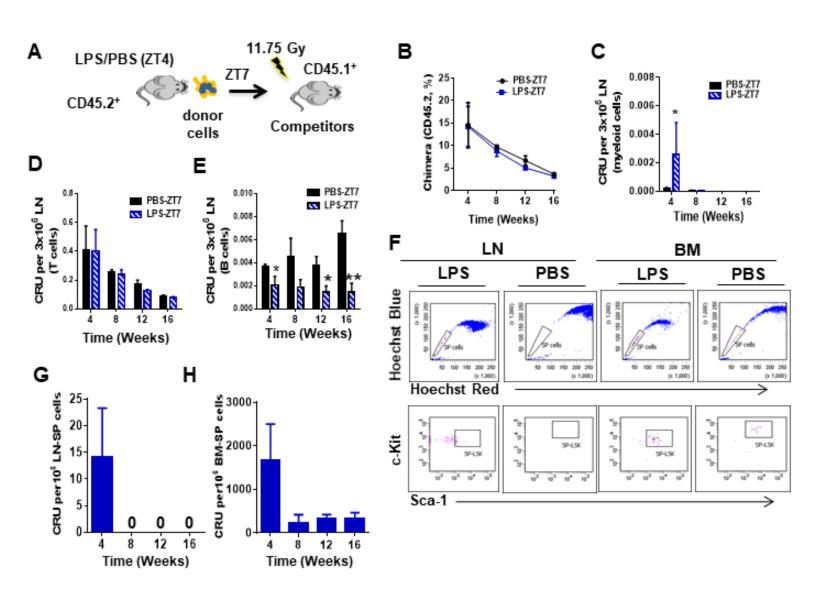




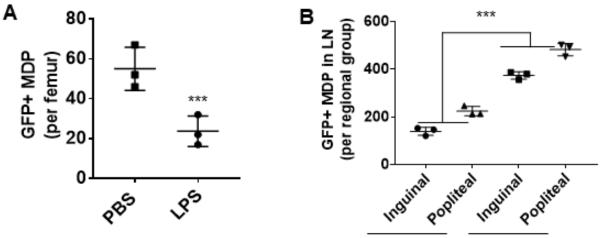






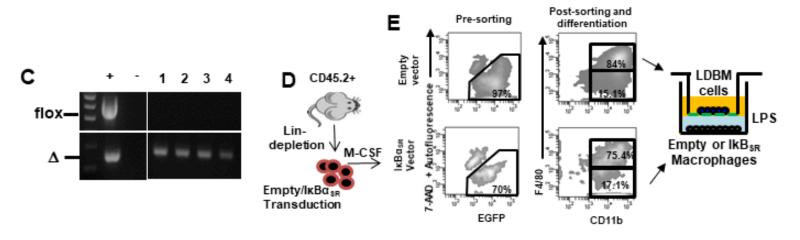


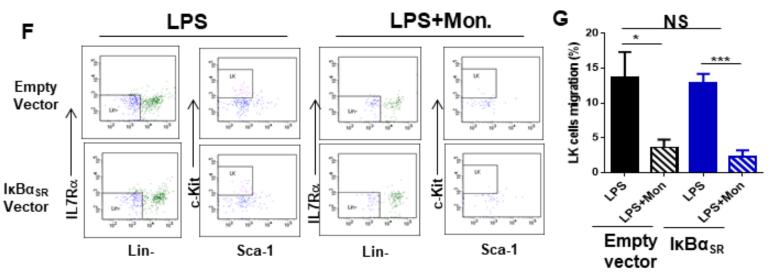
bioRxiv preprint doi: https://doi.org/10.1101/2021.01.20.427403; this version posted January 21, 2021. The copyright holder for this preprint (which was not certified by peer review) is the author/funder, who has granted bioRxiv a license to display the preprint in perpetuity. It is made available under aCC-BY 4.0 International license.

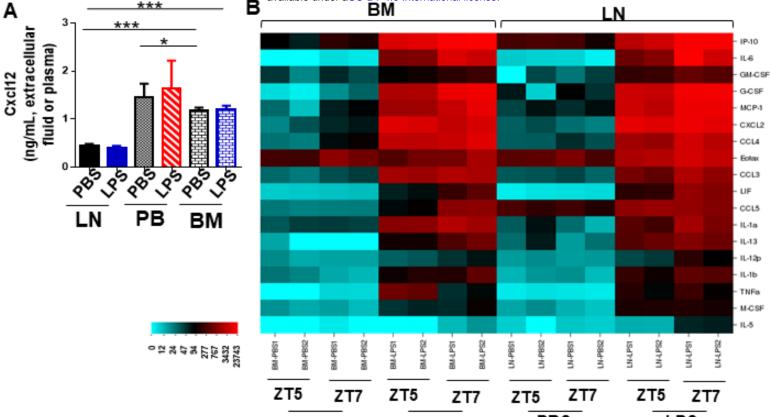


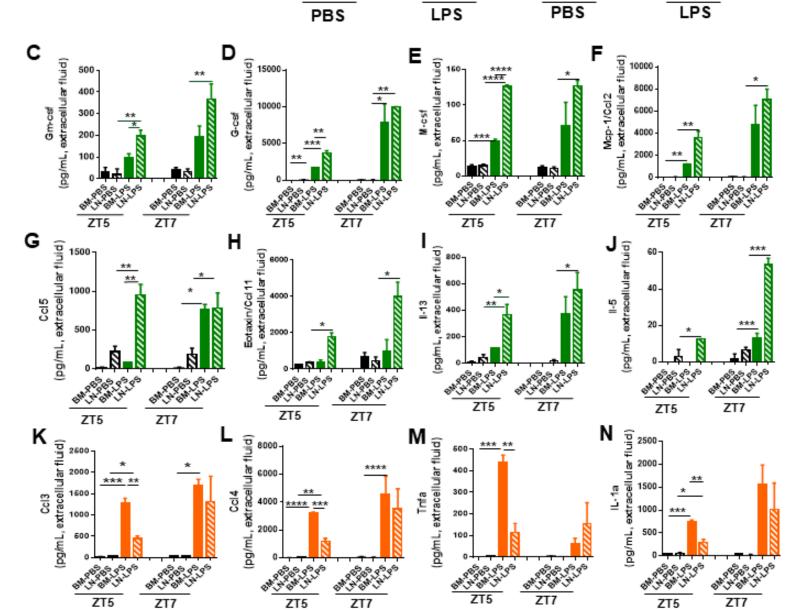




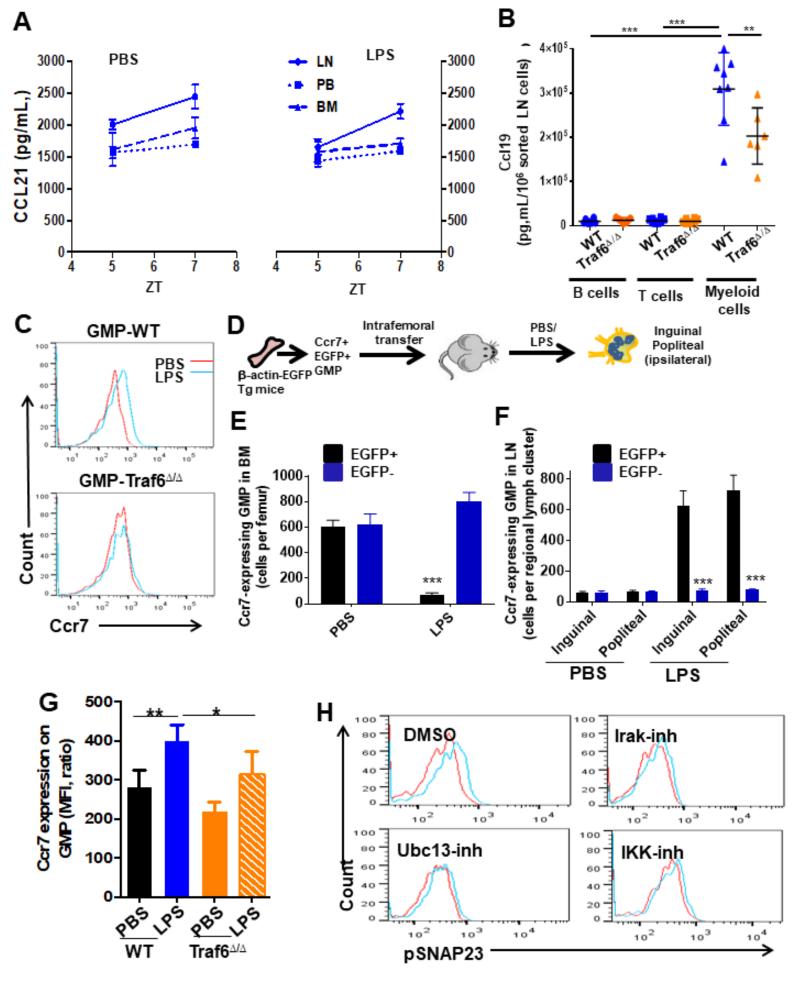


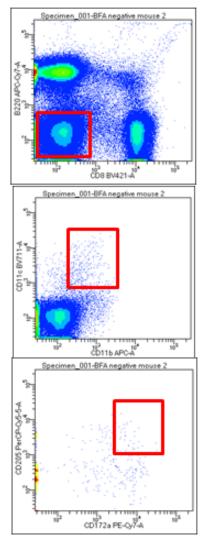






bioRxiv preprint doi: https://doi.org/10.1101/2021.01.20.427403; this version posted January 21, 2021. The copyright holder for this preprint (which was not certified by peer review) is the author/funder, who has granted bioRxiv a license to display the preprint in perpetuity. It shall be under a CC-BY 4.0 International license.





А



